Research Square

Preprints are preliminary reports that have not undergone peer review.
They should not be considered conclusive, used to inform clinical practice,
or referenced by the media as validated information.

Integrated Bioinformatics and In Vitro Metabolomics Reveal the Mechanism of Nicotinamide Metabolism-Related Genes in Uterine Corpus Endometrial Carcinoma

Pei Dong
The Fourth Affiliated Hospital of Hebei Medical University
Zixuan Su
Hebei Medical University
Lincong Zhao
Information and Communication Branch of State Grid Hebei Electic Power Co.Ltd.
Riyang Zhao
The Fourth Affiliated Hospital of Hebei Medical University
Yuyue Liu
Hebei Medical University
Zixuan Gao
Hebei Medical University
Xu Han
Hebei Medical University
Ming Ma
hinconszlc@gmail.com
The Fourth Affiliated Hospital of Hebei Medical University
Yanan Zhang
The Fourth Affiliated Hospital of Hebei Medical University

Research Article

Keywords: NMRGs, uterine corpus endometrial carcinoma, immune microenvironment, metabolomics, drug sensitivity, prognostic model

Posted Date: November 17th, 2026

DOI: https://doi.org/10.21203/rs.3.rs-11168805/v1

License: This work is licensed under a Creative Commons Attribution 4.0 International License.
Read Full License

Additional Declarations: No competing interests reported.

Title Page:

Integrated Bioinformatics and In Vitro Metabolomics Reveal the Mechanism of Nicotinamide Metabolism-Related Genes in Uterine Corpus Endometrial Carcinoma

Authors:

Pei Dong (co-first author), Department of Clinical Laboratory, The Fourth Hospital of Hebei Medical University, Shijiazhuang, Hebei, China

Zixuan Su (co-first author), College of Medical Technology, Hebei Medical University, Shijiazhuang, China

Lincong Zhao, STATE GRID HEBEI INFORMATION & TELECOMMUNICATION BRANCH, Shijiazhuang, Hebei, China

Riyang Zhao, Department of Clinical Laboratory, The Fourth Hospital of Hebei Medical University, Shijiazhuang, Hebei, China

Yuyue Liu, Clinical College, Hebei Medical University, Shijiazhuang, China

Zixuan Gao, Clinical College, Hebei Medical University, Shijiazhuang, China

Xu Han, College of Medical Technology, Hebei Medical University, Shijiazhuang, China

Ming Ma (corresponding author), Department of Clinical Laboratory, The Fourth Hospital of Hebei Medical University, Shijiazhuang, Hebei, China

Yanan Zhang (corresponding author), Department of Gynecology, The Fourth Hospital of Hebei Medical University, Shijiazhuang, Hebei, China

Contribution: Pei Dong and Zixuan Su contribute equally to this work and co-first authors.

Corresponding authors:

Yanan Zhang, Department of Gynecology, The Fourth Hospital of Hebei Medical University, Shijiazhuang, China. Email: ynzhang202210@163.com

Ming Ma, Department of Clinical Laboratory, The Fourth Hospital of Hebei Medical University, Shijiazhuang, China. Email: hinconszlc@gmail.com

Abstract

Background

Uterine corpus endometrial carcinoma (UCEC) is regarded as the second most common cancer and a leading cause of death among female cancer patients, primarily attributed to its atypical symptoms and high metastatic potential. Nicotinamide (NAM) metabolism plays an eventful role in the various tumors' progression. Nevertheless, studies on the effect of NAM in UCEC are still limited.

Methods

Transcriptional and clinical data were obtained from the TCGA database. NAM metabolism-related genes (NMRGs) were identified using the Molecular Signatures Database. Cox regression analyses (both univariate and multivariate) were performed to construct the NMRS. The Cox proportional hazards model was used to evaluate the impact of clinicopathological factors and risk scores on survival outcomes. The immune microenvironment was assessed using the ESTIMATE and CIBERSORT methods, while enrichment analysis was conducted to explore biological significance. Finally, the anticancer effect of NAM on UCEC was confirmed through functional experiments and in vitro metabolomics.

Results

Four key prognostic genes—NAXE, PARP10, PTGIS, and SLC22A13—were identified, and a correlation was found between the expression levels of these genes and clinical prognosis. Furthermore, experimental validation confirmed that NAM inhibits cell proliferation by affecting cell metabolism.

Conclusion

This study presents a novel framework for identifying prognostic biomarkers and therapeutic targets in UCEC.

Keywords

NMRGs, uterine corpus endometrial carcinoma, immune microenvironment, metabolomics, drug sensitivity, prognostic model

Introduction

Uterine corpus endometrial carcinoma (UCEC) arises from malignant epithelial tumors of the endometrium and represents the most prevalent gynecological malignancy among women, particularly affecting those in the perimenopausal and postmenopausal stages [1] [2]. With increasing life expectancy, the incidence of UCEC has progressively risen. While some cases are diagnosed early due to abnormal vaginal bleeding, the majority of patients present at advanced stages[3]. Consequently, identifying effective biomarkers for UCEC is vital for early diagnosis, targeted treatment, recurrence monitoring, and prognosis management[4, 5].

Therefore, the urgent need to develop novel and reliable biomarkers to predict prognosis, tumor progression, and drug sensitivity is critical for enabling personalized and precision-based therapies.

Nicotinamide (NAM), a water-soluble form of Vitamin B3 (niacin), is absorbed, metabolized, and excreted in the stomach or intestine, liver, and kidneys, respectively [6]. As a precursor to nicotinamide adenine dinucleotide (NAD+), NAM plays a pivotal role in various redox and non-redox reactions that regulate cellular energy metabolism [7] [8]. Previous research has shown that NAM supplementation can effectively delay aging. Senescence and cancer are closely linked, as the decline in NAD+ levels during cellular senescence leads to an increase in reactive oxygen species (ROS), which in turn promotes the accumulation of hypoxia-inducible factor-1α and triggers metabolic reprogramming. This has sparked interest in exploring the anti-tumor effects of NAM [9].

In this context, our study developed a four-gene NAM metabolism-related signature (NMRS) using data from the TCGA database. We then evaluated the predictive power of the model concerning survival outcomes, responses to immunotherapy, and the immune microenvironment. In vitro experiments demonstrated NAM's potential for anticancer and antimetastatic effects in Ishikawa cells, underscoring its therapeutic potential.

Methods

Data sources

On July 6, 2024, clinical and RNA sequencing data (RNA-seq) from 554 UCEC tumor samples and 35 adjacent normal tissues were retrieved from the TCGA database (https://portal.gdc.cancer.gov/projects/TCGA-UCEC). Two NAM metabolism-related gene sets were obtained from the Molecular Signatures Database （https://www.gsea-msigdb.org/gsea/msigdb）. The gene sets used are KEGG_NICOTINATE_AND_NICOTINAMIDE_METABOLISM (Systematic name: M19895; exact source: hsa00760; direct link: https://www.gsea-msigdb.org/gsea/msigdb/cards/KEGG_NICOTINATE_AND_NICOTINAMIDE_METABOLISM.html) and GOBP_NAD_METABOLIC_PROCESS (Systematic name: M11823; exact source: GO:0019674; direct link: https://www.gsea-msigdb.org/gsea/msigdb/cards/GOBP_NAD_METABOLIC_PROCESS). The 42 NMRGs identified from these two sets are listed in Supplementary Table S1. All procedures adhered to the ethical guidelines outlined in the Declaration of Helsinki.

Identification and enrichment analysis of differentially expressed genes (DEGs)

Differentially expressed genes (DEGs) between clusters were identified using the "limma" package, applying a threshold of |log2 fold change (FC)| > 1.5 and an adjusted P value < 0.05 [10]. Pathway and functional annotations were performed through Gene Ontology (GO) and Kyoto Encyclopedia of Genes and Genomes (KEGG) enrichment analysis using the "clusterProfiler" package in R. package [11] [12].

Construction and Validation of the Predictive NMRGS

Univariate Cox regression analysis was first applied to identify OS-related NAM metabolism-related genes (NMRGs) with a P value < 0.05. This was followed by multivariate Cox

regression analysis to isolate independent OS-related NMRGs. The expression levels and corresponding coefficients of each prognostic gene were used to calculate the risk score for UCEC patients: risk score = $h_0(t)$ * exp [Σ expression * coefficient]. Based on the median cutoff, UCEC patients were categorized into high-risk and low-risk groups for further analysis. Survival curves were used to assess the ability of the NMRGs to stratify prognoses across these groups. The reliability of the signature was evaluated using the "timeROC" package, which performed time-dependent ROC curve analysis [13].

Development and Evaluation of the NAM Metabolism-Related Nomogram

A nomogram was developed to predict the 1-, 3-, and 5-year survival probabilities of UCEC patients based on independent predictors. The accuracy and consistency of the nomogram were evaluated through calibration and time-dependent ROC curve analyses. Decision curve analysis (DCA) was conducted to assess the net benefit of the nomogram compared to a model based solely on clinical variables.

Immune Landscape, Immunotherapy Response, and Drug Sensitivity Analysis

Tumor purity, immune, stromal, and ESTIMATE scores were evaluated using the ESTIMATE algorithm. The CIBERSORT method, utilizing the LM22 gene signature matrix, was applied to assess the relative proportions of 22 immune cell types in each sample with 1000 permutations [14]. The relative infiltration of 28 immune cell subsets within the UCEC tumor microenvironment was quantified using ssGSEA. Drug sensitivity data related to NMRGs were obtained from the Genomics of Drug Sensitivity in Cancer (GDSC) database (https://www.cancerrxgene.org). The drug sensitivity analysis was performed in R using a GDSC-based R package, which retrieves GDSC drug response data internally. No manual dataset download from the GDSC website was performed [15]. Furthermore, the Absorption, Distribution, Metabolism, and Excretion (ADMET) properties of these candidate drugs were predicted using the online platform ADMETlab 2.0 (https://admetmesh.scbdd.com/service/evaluation/index). The corresponding input structures and predicted ADMET results are presented in Supplementary Data S1.

Methylation Analyses and Expression of the Prognostic Genes

UALCAN: mRNA expression and promoter methylation of PARP10, SLC22A13, NAXE (formerly APOA1BP), and PTGIS in UCEC were analysed using UALCAN (https://ualcan.path.uab.edu/cgi-bin/ualcan-res.pl).

Protein expression (immunohistochemistry) of PARP10, SLC22A13, NAXE, and PTGIS was examined using the Human Protein Atlas. Gene-specific pages are available at the following stable URLs:

PARP10: https://www.proteinatlas.org/ENSG00000178685-PARP10 /tissue

SLC22A13: https://www.proteinatlas.org/ENSG00000137833-SLC22A13 /tissue

NAXE (formerly APOA1BP): https://www.proteinatlas.org/ENSG00000163337-NAXE /tissue

PTGIS: https://www.proteinatlas.org/ENSG00000124212-PTGIS /tissue

CCK-8 Assay

Ishikawa cells (Procell China) were treated with NAM solutions at concentrations of 0, 30, 60, and 120 mM. Cell proliferation was assessed using the CCK8 assay.

Colony formation assay

Cells were trypsinized and plated at a density of 2000 per well in 6-well plates, allowing them to adhere overnight. They were then treated with varying concentrations of NAM for seven days. Following treatment, cells were fixed with 4% paraformaldehyde for 20 minutes and stained using 0.2% crystal violet. Colony morphology was captured through imaging, and the number of cell colonies was quantified.

Nontargeted metabolomics analysis using ultrahigh-performance liquid chromatography

Sample collection and preparation

Ishikawa cells were treated with NAM solutions at concentrations of 0 and 60 mM. Then, after 48 hours in culture, cells were collected and stored at -80°C before further processing for UHPLC analysis.

Metabolite extraction

According to the cell count, an isotopically labeled internal standard mixture (methanol: acetonitrile: water = 2:2:1) was added to the sample.

After 30 s of vortexing, the samples were sonicated for 15 min in an ice-water bath, incubated at -40°C for 1 h, and centrifuged at 12000 (RCF=13800 g, R=8.6 cm) rpm for 15 min at 4°C. The resulting supernatant was transferred to a fresh glass vial for analysis. A quality control (QC) sample was prepared by mixing an equal aliquot of the supernatants from all samples.

Testing

LC−MS/MS analyses were performed using a UHPLC system (Vanquish, Thermo Fisher Scientific) with a UPLC BEH Amide column (2.1 mm × 100 mm, 1.7 μm). The mobile phase consisted of 25 mmol/L ammonium acetate and 25 ammonia hydroxide in water (pH = 9.75) (A) and acetonitrile (B). The Sample tray temperature was 4°C, and the injection volume was 4 μL.

The Orbitrap Exploris 120 mass spectrometer can acquire primary and secondary mass spectrometry data using Xcalibur's control software (version 4.4, Thermo). The detailed

parameters are as follows: Sheath gas flow rate: 50 Arb, Aux gas flow rate: 15 Arb, Capillary temperature: 320 ℃, Full ms resolution: 60000, MS/MS resolution: 15000, Collision energy: SNCE 20/30/40, Spray Voltage: 3.8 kV (positive) or -3.4 kV (negative).

Statistical analysis.

Statistical analyses and graph generation were performed using R software (version 4.1.3). Survival differences between different risk groups were evaluated using Kaplan-Meier curves and the log-rank test. The Chi-square test was applied to compare categorical variables between the NMRG-high and NMRG-low groups. Spearman's correlation test was used to calculate correlation coefficients. Experimental results were plotted using GraphPad Prism. A P value of <0.05 was considered statistically significant.

3.1 Genomic and transcriptomic landscape of NMRGs

Using two gene sets related to NAM metabolism, 42 NMRGs were identified (Supplementary Table S1). A protein-protein interaction (PPI) network was constructed through the STRING database to explore the relationships among these NMRGs (Figure 1A) [16]. The PPI network of the 42 NMRGs was constructed using STRING v12.5. The network was generated with Homo sapiens as the organism and a minimum interaction score of 0.4. A co-expression network was built to understand further the interactions between NMRGs, followed by functional analysis of the associated genes (Figure 1B). Significant differences in the expression of NMRGs were observed between normal and UCEC samples (Figure 1C). The co-expression relationships of the 42 NMRGs are shown in Figure 1D. Additionally, GO and KEGG enrichment analyses were performed based on these 42 NMRGs (Figures 1E-F).

3.2 Development of NAM metabolism-related prognostic features

Univariate Cox regression analysis was used to identify NMRGs associated with UCEC in the training cohort (Figure 2A), leading to the identification of 8 prognostic NMRGs. These genes were then subjected to multivariate Cox regression analysis, which revealed four independent prognostic factors for UCEC: three risk genes (NAXE, PTGIS, SLC22A13) and one protective gene (PARP10) (Figure 2B). The prognostic model was developed based on the multivariate Cox regression coefficients and the expression levels of these four key genes. The NMRGs score for each UCEC patient was calculated as follows: NMRGs score = (0.85089 * NAXE expression) + (-0.42249 * PARP10 expression) + (0.27705 * PTGIS expression) + (3.004259 * SLC22A13 expression). Risk scores were calculated for each patient in the TCGA-UCEC cohort, and patients were categorized into high- and low-risk groups based on the median score. The distribution of NMRGs scores and survival statuses are shown in Figures 2C-D. Survival analysis revealed that patients in the low-risk group had better outcomes (Figure 2E, $P < 0.001$).

A heatmap displaying the expression of the four key genes across the two NMRGs subgroups is shown in Figure 2F. To assess the prognostic value of these genes and their impact on

overall survival (OS), separate Kaplan-Meier analyses were conducted for each gene (Supplementary Figure S1).

3.3 NMRGs risk score as an independent prognostic factor for OS

Univariate and multivariate regression analyses identified the NMRGs score as an independent prognostic factor for survival in TCGA-UCEC (Figures 3A, B). ROC curve analysis demonstrated AUC values of 0.770 at 1 year, 0.706 at 3 years, and 0.664 at 5 years, indicating that the NMRGs score has strong predictive power for patient survival. Notably, the NMRGs risk score outperformed other clinicopathological factors in predicting survival outcomes for UCEC patients (Figures 3C-E).

A significant correlation was found between the risk score and the four NMRGs, and clinicopathological factors (Supplementary Figure S2).

3.4 Development of nomograms based on NMRGs scores and WHO grades

To improve the clinical applicability of the risk model, a nomogram incorporating risk scores and clinicopathological features was developed to predict 1-, 3-, and 5-year OS (Figure 4A). Calibration plots based on the NMRGs nomogram showed strong agreement between actual and predicted OS probabilities at these time points (Figure 4B). The AUC values at 1, 3, and 5 years were 0.801, 0.851, and 0.821, respectively, validating the nomogram's predictive accuracy (Figure 4C). Both univariate and multivariate regression analyses confirmed the nomogram as an independent risk factor for survival (Figures 4E-F). Decision curve analysis (DCA) further assessed the nomogram's clinical utility. Compared to models based only on clinical characteristics, this comprehensive nomogram provided greater net benefit, potentially improving clinical management (Figure 4G).

3.5 DEGs, function enrichment analysis, and somatic mutations in two risk groups

Differential expression analysis identified 218 DEGs between the high- and low-risk groups (Figures 5A-B). GO and KEGG enrichment analyses were performed on these DEGs. Additionally, somatic mutations in both risk groups were analyzed. Figures 6A-B show the top 10 most frequently mutated genes in each group. In the high-risk group, 244 of 250 samples (97.6%) contained mutations, while in the low-risk group, 258 of 261 samples (98.85%) had mutations. The most frequently mutated genes in the high-risk group were PTEN, ARID1A, PIK3CA, TP53, and TTN, while in the low-risk group, the top five were PTEN, PIK3CA, ARID1A, TTN, and PIK3R1.

3.6 Identification of Immune Landscape

The ESTIMATE and CIBERSORT algorithms were used to analyze the tumor microenvironment (TME). ESTIMATE analysis revealed that the low-risk group had high ImmuneScores, StromalScores, and ESTIMATEScores, along with lower TumorPurity ($P < 0.05$) (Figure 7A). The CIBERSORT algorithm assessed the relative proportions of 22 immune cell types in UCEC samples from the TCGA dataset (Figure 7B). The results

revealed significant differences in the immune landscape between the low-risk and high-risk groups. Compared with the high-risk group, the low-risk group exhibited marked immune activation characteristics, with significantly increased infiltration of specific immune subsets. Specifically, the proportions of Plasma cells and T cells regulatory (Tregs) were significantly elevated in the low-risk group. Conversely, the proportions of Dendritic cells resting and Neutrophils were significantly higher in the high-risk group (Figure 7C). These findings suggest a potential association between risk scores and immune infiltration, which may influence UCEC prognosis.

Overall, these results indicate that the NMRGs risk model is linked to immune infiltration and reflects the immune profile of UCEC patients.

Additionally, ssGSEA was used to calculate the scores for 28 immune cell types and analyze their differential expression across the two risk groups. The relationships between these 28 immune cells were also explored (Figure 7D-E).

3.7 Drug sensitivity analysis

The IC50 value was used as an indicator of chemotherapy sensitivity for eleven commonly used small-molecule drugs in UCEC patients. Figure 8 shows that the IC50 values for DMOG, JNK.9L, and ABT.263 were significantly higher in the low-risk group, while the IC50 values for NVP.BEZ235, Z.LLNle.CHO, Metformin, Nutlin.3a, SB.216763, MK.2206, Temsirolimus, and CEP.701 were lower in the high-risk group (Figure 8A). Supplementary Figure S3 illustrates the correlation between the risk score and drug sensitivity. These results suggest that UCEC patients in different risk subgroups have varied responses to different anti-tumor agents, highlighting the potential for personalized treatment to benefit patients.

We analyzed the ADMET of these candidate drugs using the data source of ADMETlab 2.0. The observations suggested that the JNK.9L compound is the most promising drug (Figure 8B). These candidate drugs have the potential to be therapeutic drugs in UCEC.

3.8 Validation of NMRGs

Validation of mRNA and protein expression levels of NMRGs was conducted using the UALCAN and HPA databases. PTGIS showed reduced expression in primary tumor tissues compared to normal tissues, whereas other genes, such as PARP10, SLC22A13, and NAXE(APOA1BP), exhibited elevated expression (Figure 9A). Interestingly, the methylation levels of the promoter regions of the prognostic genes (PARP10) were inversely correlated with their expression levels (Figure 9B). Furthermore, protein expression levels of several prognostic genes were confirmed (Figure 9C), which aligned with the observed gene expression patterns.

3.9 NAM Suppresses Cell Proliferation in UCEC Cells

The CCK-8 assay and plate colony formation results demonstrated a significant reduction in cell proliferation in the experimental groups compared to the control group (Figure 10A-B).

3.10 Nontargeted metabolomics analysis between the control and NAM-treated groups

3.10.1. Multivariate statistical analysis

To investigate the metabolic changes induced by NAM treatment, non-targeted metabolomics analysis was conducted using LC-MS/MS after exposing cells to different concentrations of NAM (0, 60mM) for 48 hours. Following preprocessing and log transformation of the raw data, multivariate analysis was performed. The unsupervised PCA score plots did not show a distinct separation between the groups in both positive- and negative-ion modes (Figure 11A). However, OPLS-DA, a more suitable method for distinguishing origins when multiple factors influence metabolite profiles, was applied to refine the analysis. The OPLS-DA score plots revealed a clear separation between the two groups in both modes (Figure 11B).

To assess the validity of the model, permutation tests with 200 iterations were performed, confirming that the OPLS-DA model was not overfitted in either mode (positive-ion: $p < 0.05$; negative-ion: $p < 0.05$; Figure 11C). These findings indicated that the metabolic alterations between the control and NAM-treated groups were statistically significant.

3.10.2. Analysis of differential metabolites

Differential metabolite analysis revealed a total of 283 metabolites with significant differences between the two groups in the positive-ion mode. Of these, 142 metabolites were downregulated, while 141 were upregulated (Figure 12A, Supplementary Table S2). These DMs were classified into 12 categories (Figure 12C), with lipids and lipid-like molecules (25.47%) and organoheterocyclic compounds (21.16%) being the largest groups. In the negative-ion mode, 128 DMs were identified, including 54 downregulated and 74 upregulated metabolites (Figure 12B, Supplementary Table S3). The majority of these were also lipids and lipid-like molecules (24.07%) or organoheterocyclic compounds (16.2%) (Figure 12D).

The top 20 most significantly differential metabolites were selected based on P values and presented in a stick plot. A correlation heat map was also used to visualize the relationship between metabolite classes and their contents (Figure 12E-F).

Strong correlations were observed within the different metabolite groups, such as between Hexanoylcarnitine and octanoylcarnitine (Supplementary Figure S4A-B). These results suggest a strong interconnectedness among different metabolites. Overall, the analysis confirmed significant metabolic differences between the control and NAM-treated groups.

3.10.3 Metabolic enrichment analysis and pathway analysis

In positive-ion mode, pathway enrichment analysis based on metabolic sets revealed that these DMs were primarily enriched in ABC transport (22.22%) and nucleotide metabolism (22.22%), followed by glycerophospholipid metabolism (16.67%) and arginine and proline metabolism (16.67%), as illustrated in Figure 13A. Subsequently, differential abundance score analysis was conducted to evaluate the overall changes in all DMs enriched in the same pathway.

The results indicated that pathways such as sphingolipid metabolism and the sphingolipid signaling pathway exhibited a significant upregulation trend (Figure 13B).

Likewise, in negative-ion mode, these DMs were mainly enriched in nucleotide metabolism (17.14%) and pyrimidine metabolism (17.14%) (Figure 13C). Differential abundance score analysis further demonstrated that glycosylphosphatidylinositol (GPI)-anchor biosynthesis, pathogenic Escherichia coli infection, biosynthesis of unsaturated fatty acids, and autophagy-related pathways were significantly upregulated (Figure 13D).

KEGG annotation analysis has primarily identified the pathways associated with differential metabolites. However, to comprehensively analyze the substance changes induced by experimental conditions and their effects on the involved pathways, it is essential to assess the impact of differential metabolites on these pathways. By performing a detailed analysis of pathways containing the differential metabolites, including enrichment and topological analysis, we can further identify key pathways with the strongest correlation to metabolite variations. As shown in Figure 14A-B, among 20 metabolic pathways, only 4 were significantly enriched ($p < 0.05$, impact > 0.1), namely 'arginine and proline metabolism,' 'glycine, serine, and threonine metabolism,' 'glycerophospholipid metabolism,' and 'purine metabolism'. Similarly, 19 metabolic pathways were identified in the negative-ion mode, of which 3 pathways showed significant enrichment ($p < 0.05$, impact > 0.1). The predominant pathways were 'pyrimidine metabolism,' 'citrate cycle,' and 'glyoxylate and dicarboxylate metabolism' (Figures 14C, D).

Discussion

UCEC represents the most prevalent malignant tumor within the female reproductive system[17]. Currently, its global incidence is rising annually, posing a significant threat to women's health. Early detection and treatment yield a 5-year survival rate of 90%[18, 19]. Conversely, the presence of lymph nodes or distant metastasis drastically reduces this survival rate. Consequently, investigating the pathogenesis of this cancer and identifying early diagnostic markers is essential.

Current research on prognostic risk prediction models for UCEC is expanding annually. While the role of metabolism in cancer progression has been acknowledged, few studies have focused on developing metabolic-based prognostic models [20]. Notably, the prognostic characteristics associated with four metabolism-related genes have been shown to accurately predict survival outcomes in UCEC patients. These metabolism-related genes may serve as both biomarkers and potential therapeutic targets for this patient population.

NAXE functions as an epimerase and serves as a critical component of the dual-enzyme NAD(P)HX repair system. A deficiency in NAXE has been linked to severe neurometabolic and neuroinflammatory disorders [21]. We found that elevated NAXE expression is associated with increased risk, suggesting that enhanced NAD(P)H repair capacity may support the metabolic demands of aggressive UCEC tumors.

PARP10, a mono ADP ribosyltransferase, exhibits catalytic activity that influences several pathways, notably the regulation of cancer cell proliferation and tumor metastasis [22].

Prostacyclin synthase (PTGIS), also referred to as PGIS belongs to the cytochrome P450 superfamily and catalyzes the conversion of arachidonic acid into PGI2. Numerous studies indicate that PTGIS is instrumental in the onset and progression of various cancers, including colon, breast, and lung cancers [23] [24].

SLC22A13 gene encodes the organic anion transporter 10 (OAT10). Research by Kang et al. demonstrated that both mRNA and protein levels of SLC22A13 were significantly reduced in ccRCC, with its expression serving as a reliable prognostic indicator for patients [25]. The four selected NMRGs play significant roles in the regulation of metabolic processes in cancer, either directly or indirectly.

The NMRG-based risk score demonstrated robust predictive performance, with 1-, 3-, and 5-year AUC values of 0.770, 0.706, and 0.664, respectively—outperforming traditional clinicopathological factors. Integrating this risk score into a nomogram further enhanced clinical utility, as evidenced by calibration plots, time-dependent ROC curves, and decision curve analysis. These findings indicate that the NMRG signature serves as a practical tool for UCEC risk stratification and clinical decision-making.

A central focus of this study was the relationship between the NMRG signature and the tumor immune microenvironment. ESTIMATE analysis revealed that the low-risk group exhibited higher ImmuneScores, StromalScores, and ESTIMATEScores, alongside lower TumorPurity, suggesting richer immune infiltration within the TME. CIBERSORT analysis further showed significantly higher infiltration proportions of plasma cells and regulatory T cells (Tregs) in the low-risk group, whereas the high-risk group displayed significantly increased proportions of resting dendritic cells and neutrophils. Plasma cells contribute to anti-tumor humoral immunity through antibody secretion; resting dendritic cells may promote immune escape due to limited antigen-presenting capabilities; and neutrophils can drive tumor progression by secreting pro-angiogenic factors (such as VEGF) and immunosuppressive mediators. In summary, the immunosuppressive infiltration pattern dominated by resting dendritic cells and neutrophils in the high-risk group provides a plausible immunological explanation for the poorer prognosis observed in this patient population. Our experiments have validated NAM's inhibitory effect on UCEC cell proliferation. We further studied the metabolic characteristics of NAM in Ishikawa cells. Metabolomics is a powerful approach to studying metabolic processes, identifying key biomarkers, and uncovering metabolic mechanisms. In this study, non-targeted metabolic analysis was performed to elucidate the metabolic profiles of NAM. The results revealed significant metabolic changes between the two groups. The pathways most strongly associated with metabolite differences were ‘glycerophospholipid metabolism’ and ‘pyrimidine metabolism.’ These findings suggest that these pathways play a crucial role

in metabolic regulation. Overall, our results indicate that NAM is involved in the modulation of Ishikawa metabolism.

In summary, this study presents the first comprehensive characterization of NAM metabolism-related genes (NMRGs) in UCEC, integrating bioinformatics, immune profiling, drug sensitivity assessment, and experimental metabolomics. We established a four-gene NMRGs signature that independently predicts patient prognosis and developed a nomogram to enhance its clinical utility. Furthermore, our analysis links this signature to distinct immune landscapes and chemotherapeutic sensitivities, while in vitro experiments and metabolomics reveal that NAM suppresses UCEC proliferation by perturbing nucleotide and phospholipid metabolism. These findings advance the understanding of metabolic reprogramming in endometrial carcinogenesis and offer a foundation for personalized therapeutic strategies.

1. Siegel, R.L., K.D. Miller, and A. Jemal, *Cancer statistics, 2020.* CA Cancer J Clin, 2020. **70**(1): p. 7-30.
2. Prat, J., et al., *Endometrial carcinoma: pathology and genetics.* Pathology, 2007. **39**(1): p. 72-87.
3. De Nola, R., et al., *The Crowded Crosstalk between Cancer Cells and Stromal Microenvironment in Gynecological Malignancies: Biological Pathways and Therapeutic Implication.* Int J Mol Sci, 2019. **20**(10).
4. Group, S.G.O.C.P.E.C.W., et al., *Endometrial cancer: a review and current management strategies: part I.* Gynecol Oncol, 2014. **134**(2): p. 385-92.
5. Group, S.G.O.C.P.E.C.W., et al., *Endometrial cancer: a review and current management strategies: part II.* Gynecol Oncol, 2014. **134**(2): p. 393-402.
6. Surjana, D., G.M. Halliday, and D.L. Damian, *Role of nicotinamide in DNA damage, mutagenesis, and DNA repair.* J Nucleic Acids, 2010. **2010**.
7. Hwang, E.S. and S.B. Song, *Nicotinamide is an inhibitor of SIRT1 in vitro, but can be a stimulator in cells.* Cell Mol Life Sci, 2017. **74**(18): p. 3347-3362.
8. Song, S.B., et al., *Diverse therapeutic efficacies and more diverse mechanisms of nicotinamide.* Metabolomics, 2019. **15**(10): p. 137.
9. DeBerardinis, R.J. and N.S. Chandel, *Fundamentals of cancer metabolism.* Sci Adv, 2016. **2**(5): p. e1600200.
10. Ritchie, M.E., et al., *limma powers differential expression analyses for RNA-sequencing and microarray studies.* Nucleic Acids Res, 2015. **43**(7): p. e47.
11. Harris, M.A., et al., *The Gene Ontology (GO) database and informatics resource.* Nucleic Acids Res, 2004. **32**(Database issue): p. D258-61.
12. Kanehisa, M. and S. Goto, *KEGG: kyoto encyclopedia of genes and genomes.* Nucleic Acids Res, 2000. **28**(1): p. 27-30.
13. Blanche, P., J.F. Dartigues, and H. Jacqmin-Gadda, *Estimating and comparing time-dependent areas under receiver operating characteristic curves for censored event times with competing risks.* Stat Med, 2013. **32**(30): p. 5381-97.
14. Chen, B., et al., *Profiling Tumor Infiltrating Immune Cells with CIBERSORT.* Methods Mol Biol, 2018. **1711**: p. 243-259.

15. Yang, W., et al., *Genomics of Drug Sensitivity in Cancer (GDSC): a resource for therapeutic biomarker discovery in cancer cells.* Nucleic Acids Res, 2013. **41**(Database issue): p. D955-61.
16. Szklarczyk, D., et al., *The STRING database in 2021: customizable protein-protein networks, and functional characterization of user-uploaded gene/measurement sets.* Nucleic Acids Res, 2021. **49**(D1): p. D605-D612.
17. Liu, J., et al., *Pyroptosis-related lncRNAs are potential biomarkers for predicting prognoses and immune responses in patients with UCEC.* Mol Ther Nucleic Acids, 2022. **27**: p. 1036-1055.
18. Yen, M.S., et al., *Clinicopathologic Features and Treatment Outcomes in Patients with Stage I, High-Risk Histology or High-Grade Endometrial Cancer after Primary Staging Surgery: A Taiwanese Gynecologic Oncology Group Study.* J Clin Med, 2018. **7**(9).
19. Miller, M.D., et al., *An integrated prediction model of recurrence in endometrial endometrioid cancers.* Cancer Manag Res, 2019. **11**: p. 5301-5315.
20. Yang, S., et al., *Identification and Validation of Nicotinamide Metabolism-Related Gene Signatures as a Novel Prognostic Model for Hepatocellular Carcinoma.* Onco Targets Ther, 2024. **17**: p. 423-438.
21. Manor, J., et al., *NAXE deficiency: A neurometabolic disorder of NAD(P)HX repair amenable for metabolic correction.* Mol Genet Metab, 2022. **136**(2): p. 101-110.
22. Zhou, Z., et al., *Depletion of PARP10 inhibits the growth and metastatic potential of oral squamous cell carcinoma.* Front Genet, 2022. **13**: p. 1035638.
23. Peng, H., et al., *Hypoxia-hindered methylation of PTGIS in endometrial stromal cells accelerates endometriosis progression by inducing CD16(-) NK-cell differentiation.* Exp Mol Med, 2022. **54**(7): p. 890-905.
24. Ding, H., et al., *Validating the role of PTGIS gene in colorectal cancer by bioinformatics analysis and in vitro experiments.* Sci Rep, 2023. **13**(1): p. 16496.
25. Kang, W., et al., *The SLC Family Are Candidate Diagnostic and Prognostic Biomarkers in Clear Cell Renal Cell Carcinoma.* Biomed Res Int, 2020. **2020**: p. 1932948.

Declarations

Ethical Approval and Accordance

Not applicable. This study used publicly available, de-identified datasets from the TCGA database. No identifiable human participants, human tissues, or animal subjects were involved. Therefore, ethical approval and consent to participate were not required.

Consent to participate

Not applicable. This study used publicly available, de-identified datasets and did not involve direct participation of identifiable human participants.

Consent for publish

Not applicable. This study used publicly available, de-identified datasets and did not involve identifiable human images or materials. Therefore, consent for publication is not required.

FUNDING

This study was supported by the Medical Science Research Project of Hebei (No. 20240360), Undergraduate Innovation Experiment Program (USIP2025328), Government-funded Program for Clinical Medicine Talents (ZF2025191), and Hebei Natural Science Foundation (H2024206074)

CONFLICT OF INTERESTS

The authors declare that there is no conflict of interest.

DATA AVAILABILITY STATEMENT

All data generated or analyzed during this study are included in this published article and its supplementary information files.

TCGA-UCEC: Clinical and RNA sequencing data were retrieved from The Cancer Genome Atlas (TCGA) via the Genomic Data Commons (GDC) Data Portal: https://portal.gdc.cancer.gov/projects/TCGA-UCEC.

MSigDB: Two NAM metabolism-related gene sets were obtained from the Molecular Signatures Database (MSigDB) (https://www.gsea-msigdb.org/gsea/msigdb). The gene sets used are KEGG_NICOTINATE_AND_NICOTINAMIDE_METABOLISM (Systematic name: M19895; exact source: hsa00760; direct link: https://www.gsea-msigdb.org/gsea/msigdb/cards/KEGG_NICOTINATE_AND_NICOTINAMIDE_METABOLISM.html) and GOBP_NAD_METABOLIC_PROCESS (Systematic name: M11823; exact source: GO:0019674; direct link: https://www.gsea-msigdb.org/gsea/msigdb/cards/GOBP_NAD_METABOLIC_PROCESS). The 42 NMRGs identified from these two sets are listed in Supplementary Table S1.

STRING: The PPI network of the 42 NMRGs was constructed using STRING v12.5. The network was generated with Homo sapiens as the organism and a minimum interaction score

of 0.4. Direct link to the STRING network/analysis page: https://string-db.org/cgi/network?pollingId=bILEty0vcRvm&sessionId=bkN5qHmiJPch

GDSC: Drug sensitivity data related to NMRGs were obtained from the Genomics of Drug Sensitivity in Cancer (GDSC) database (https://www.cancerrxgene.org). The drug sensitivity analysis was performed in R using a GDSC-based R package, which retrieves GDSC drug response data internally. No manual dataset download from the GDSC website was performed.

UALCAN: mRNA expression and promoter methylation of PARP10, SLC22A13, NAXE, and PTGIS in UCEC were analysed using UALCAN (https://ualcan.path.uab.edu/cgi-bin/ualcan-res.pl).

HPA: Protein expression of PARP10, SLC22A13, NAXE, and PTGIS was examined using the Human Protein Atlas. Gene-specific pages are available at the following stable URLs:

PARP10: https://www.proteinatlas.org/ENSG00000178685-PARP10/tissue

SLC22A13: https://www.proteinatlas.org/ENSG00000137833-SLC22A13/tissue

NAXE (formerly APOA1BP): https://www.proteinatlas.org/ENSG00000163337-NAXE/tissue

PTGIS: https://www.proteinatlas.org/ENSG00000124212-PTGIS/tissue

ADMETlab 2.0: As ADMETlab 2.0 is a dynamic online prediction web server rather than a static database, it does not assign permanent accession numbers to individual queries. We have therefore provided the direct URL to the specific evaluation module used (https://admetmesh.scbdd.com/service/evaluation/index) and noted that the specific input

structures and prediction results are fully disclosed in Supplementary Data S1 of the revised manuscript.

Author Contributions

Pei Dong: Conceptualization, Formal analysis, Project administration, Writing - original draft

Zixuan Su: Visualization, Editing

Lincong Zhao: Resources, Software

Riyang Zhao: Resources, Software

Yuyue Liu: Validation

Zixuan Gao: Writing - review & editing

Xu Han: Investigation

Ming Ma: Methodology， Formal analysis

Yanan Zhang: Funding acquisition, Writing - review & editing

Figure brief title and description

Figure1
Title: Evaluation of NMRGs in UCEC.
Description: (A) PPIs between NMRGs using the STRING database. (B) Analysis of DEGs and their co-expressed genes via GeneMANIA. (C)Heatmap displaying the expression of 42 NMRGs in UCEC and normal tissue samples using the TCGA database. (D)Correlation analysis between 42 NMRGs. (E, F) GO and KEGG pathway analysis of NMRGs.

Figure2
Title: Development and assessment of prognostic signature based on NMRGs in the TCGA dataset.
Description: (A, B) Univariate and multivariate Cox regression analyses were performed to assess the prognostic values of the NMRGs with regard to UCEC.(C–E) Risk score distribution (C), survival status of each patient (D), and Kaplan–Meier curves of low- and

high-risk subgroups based on risk score (E). (F) Heatmaps of the prognostic 4-gene signature in the TCGA database.

Figure3

Title: Independent prognostic analysis of risk scores.

Description: (A) Prognostic effect analysis of risk score and clinical features in UCEC with univariate Cox regression analysis. (B) Independent prognostic effect analysis of risk score and traditional prognostic clinical features in UCEC with multivariate Cox regression analysis. (C-E) Receiver operating characteristic analysis of UCEC risk scores and other prognostic clinical characteristics to predict the 1-, 3-, and 5-year survival rate of UCEC patients.

Figure4

Title: Establishment of a predictive nomogram.

Description: (A) Nomogram predicting the 1-, 2-, and 3-year survival rates for UCEC patients. (B)

Calibration curves for the nomogram prediction validation cohort of UCEC patient survival (x-axis: the predicted survival probability; y-axis: the actually observed survival probability). (C-E) Receiver operating characteristic analysis of the UCEC nomogram and other prognostic clinical characteristics to predict the 1-, 3-, and 5-year survival rates of UCEC patients. (F) Assessing the relationship between risk scores and clinical factors with OS using a forest plot of the univariate Cox test results. (G) The independent risk factors for OS were determined using a forest plot of the multivariate Cox analysis results. OS, overall survival; AUC, area under the curve; CI, confidence interval. (H) DCA curves of the clinicopathological indicators and this nomogram.

Figure5

Title: Analysis of the differentially expressed genes (DEGs) and functional enrichment analysis in different NMRGs risk scores.

Description: (A) Volcano plot of the distribution of DEGs between the NMRGs-high and NMRGs-low risk groups in the TCGA cohort. (B) Heatmap of DEG expression between the NMRGs-high and NMRGs-low risk groups. (C, D) The GO and KEGG enrichment analyses of signaling pathways; the colour of the dot represents the p-value.

Figure6

Title: Comparison of somatic mutations between different NMRG subtypes.

Description: Oncoprint visualization of the top ten most frequently mutated genes in the high-risk group (A) and low-risk group (B).

Figure7

Title: The immune landscape between the NMRGs-high and NMRGs-low groups.

Description: (A) Violin plots of the stromal score, immune score, ESTIMATE score, and tumour purity between the NMRGs-high and NMRGs-low risk groups. (B) Relative percentage of immune infiltration in the NMRGs-high and NMRGs-low risk groups. (C) The fraction of 22 immune cells in the low- and high-risk groups, calculated by the CIBERSORT algorithm. (D) The fraction of 28 immune cells in the low- and high-risk groups, calculated by the ssGSEA algorithm. (E) Heatmap of the correlations among different immune cells. Blue and red illustrate positive and negative associations, respectively. ns, $P>0.05$; *, $P<0.05$; **, $P<0.01$; ***, $P<0.001$.

Figure8

Title: Drug sensitivity analysis in low- and high-risk groups.

Description: (A) The IC50 value exhibits a significant difference between the low- and high-risk groups among NVP.BEZ235, Z.LLNle.CHO, DMOG, JNK.9L, Metformin, Nutlin.3a, SB.216763, MK.2206, ABT.263, Temsirolimus, CEP.701. (B) ADMET attributes of potential therapeutic drugs.

Figure9

Title: Validation of NMRGs.

Description: Validation of the mRNA expression levels (A) and promoter methylation levels (B) of NMRGs via the UALCAN database. Validation of the protein expression levels via IHC in the HPA database (C).

Figure10

Title: NAM regulates cell proliferation.

Description: (A-B) A CCK-8 assay and plate colony formation assay were used to assess the proliferation ability of Ishikawa cells cultured with 0, 30, 60, or 120 mM NAM for 48 hours.

Figure11

Title: Multivariate Analysis of Untargeted Metabolic Profiling.

Description: (A) Principal Component Analysis (PCA) score plots for both positive-ion and negative-ion modes. (B) Orthogonal Partial Least Squares Discriminant Analysis (OPLS-DA) score plots in both ionization modes. (C) Histogram of the permutation test results for the OPLS-DA model.

Figure12

Title: Differential metabolites (DMs) between control and NAM-treated groups by nontargeted metabolic analysis.

Description: (A, B) Volcano plot analysis of DMs with VIP value > 1 and P value <0.05 in both modes. (C, D) Distribution of all DMs in both modes. (E, F) Heatmap of hierarchical cluster analysis of the top 30 upregulated and downregulated DMs in both modes.

Figure13

Title: KEGG enrichment analysis of differential metabolites (DMs) by nontargeted metabolic analysis.

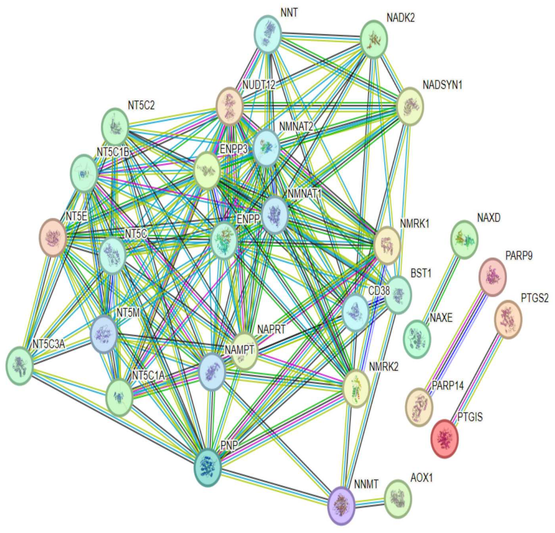
Description: (A, C) Enrichment analysis of DMs. (B, D) Differential abundance score analysis of DMs. * $P < 0.05$, ** $P < 0.01$, *** $P < 0.001$.

Figure14

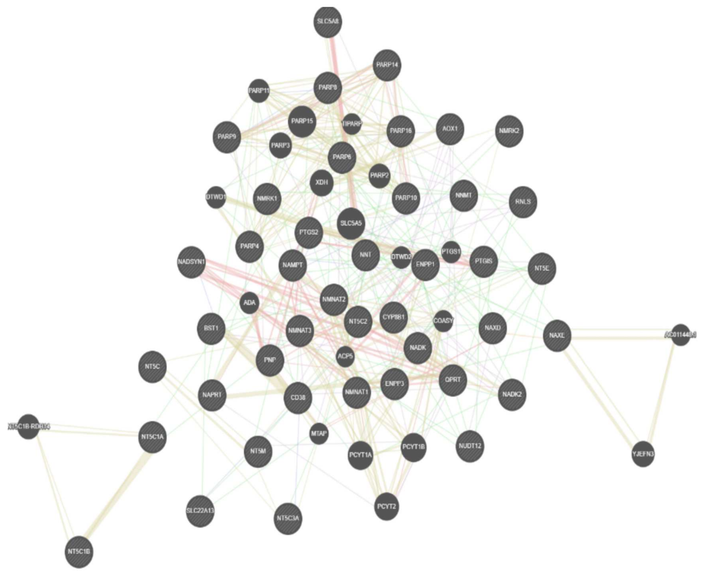
Title: KEGG pathway analysis of differential metabolites (DMs) based on nontargeted metabolic analysis.

Description: (A, C) Bubble plots illustrate pathways as circles, where size represents impact value and color denotes the P value. (B, D) Treemaps display pathways as rectangles, with both attributes conveying the same metrics.

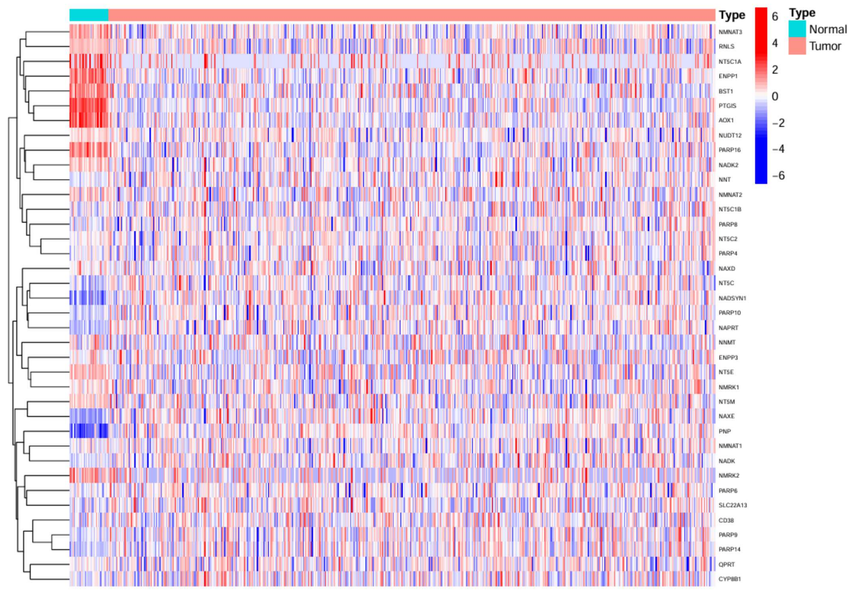
(A)


NNT
NADK2
NUDT12
NADSYN1
NT5C2
NMNAT2
ENPP3
NT5C1B
NMNAT1
NT5E
ENPP
NT5C
NMRK1
NAXD
PARP9
BST1
CD38
PTGS2
NT5M
NAXE
NAPRT
NT5C3A
NAMPT
NT5C1A
NMRK2
PARP14
PTGIS
PNP
NNMT
AOX1

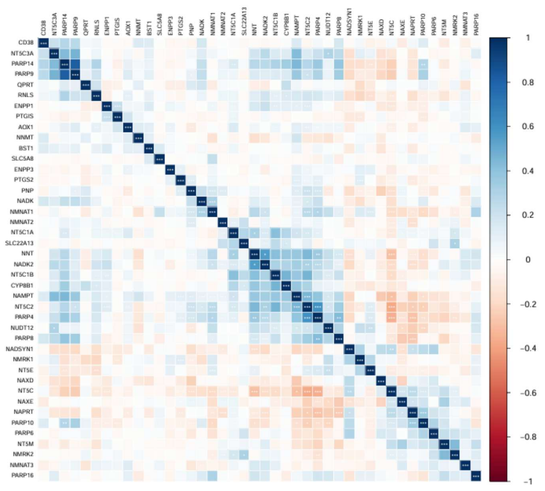
(B)



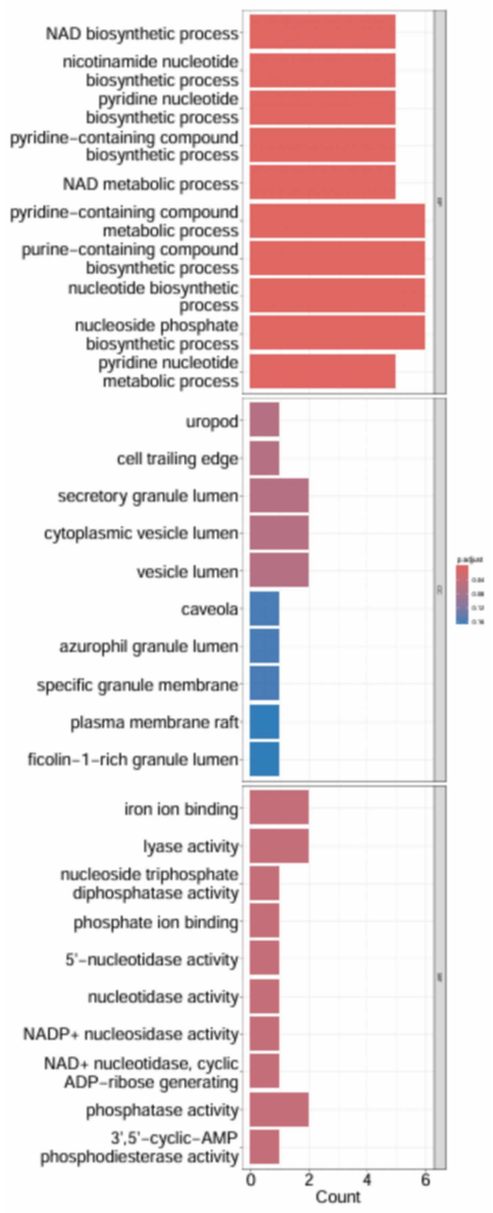
(C)


Type
Normal
Tumor
6
4
2
0
−2
−4
−6

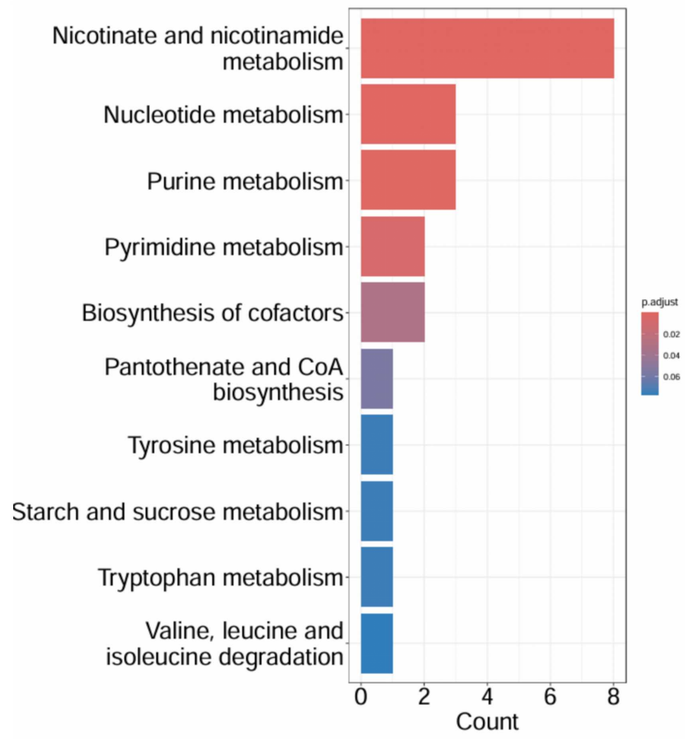
(D)


1
0.8
0.6
0.4
0.2
0
−0.2
−0.4
−0.6
−0.8
−1

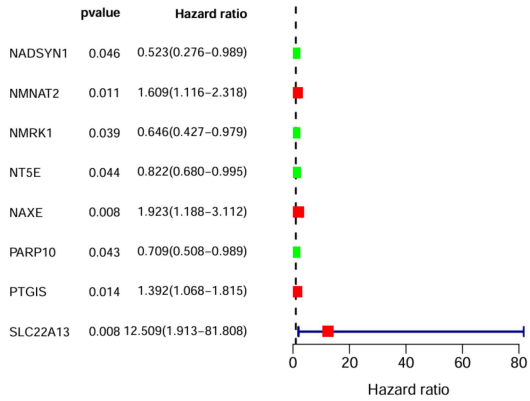
(E)


NAD biosynthetic process
nicotinamide nucleotide biosynthetic process
pyridine nucleotide biosynthetic process
pyridine-containing compound biosynthetic process
NAD metabolic process
pyridine-containing compound metabolic process
purine-containing compound biosynthetic process
nucleotide biosynthetic process
nucleoside phosphate biosynthetic process
pyridine nucleotide metabolic process
uropod
cell trailing edge
secretory granule lumen
cytoplasmic vesicle lumen
vesicle lumen
caveola
azurophil granule lumen
specific granule membrane
plasma membrane raft
ficolin-1-rich granule lumen
iron ion binding
lyase activity
nucleoside triphosphate diphosphatase activity
phosphate ion binding
5'-nucleotidase activity
nucleotidase activity
NADP+ nucleosidase activity
NAD+ nucleotidase, cyclic ADP-ribose generating
phosphatase activity
3',5'-cyclic-AMP phosphodiesterase activity
0
2
4
6
Count
p.adjust

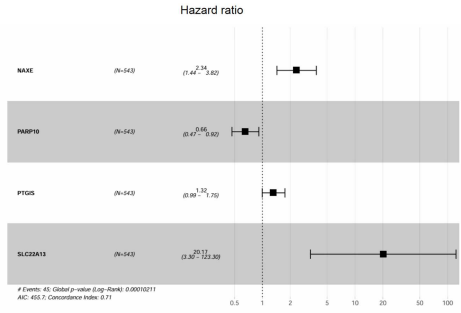
(F)


Nicotinate and nicotinamide metabolism
Nucleotide metabolism
Purine metabolism
Pyrimidine metabolism
Biosynthesis of cofactors
Pantothenate and CoA biosynthesis
Tyrosine metabolism
Starch and sucrose metabolism
Tryptophan metabolism
Valine, leucine and isoleucine degradation
0
2
4
6
8
Count
p.adjust
0.02
0.04
0.06

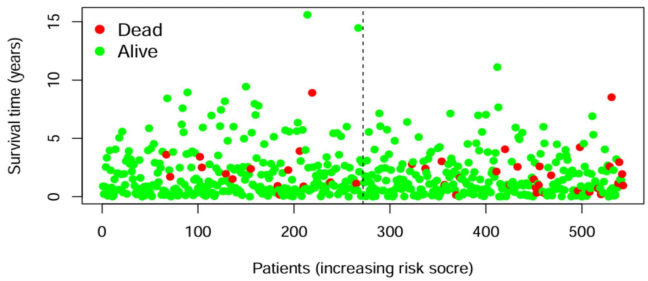
(A)


pvalue
Hazard ratio
NADSYN1 0.046 0.523(0.276−0.989)
NMNAT2 0.011 1.609(1.116−2.318)
NMRK1 0.039 0.646(0.427−0.979)
NT5E 0.044 0.822(0.680−0.995)
NAXE 0.008 1.923(1.188−3.112)
PARP10 0.043 0.709(0.508−0.989)
PTGIS 0.014 1.392(1.068−1.815)
SLC22A13 0.008 12.509(1.913−81.808)
0 20 40 60 80
Hazard ratio

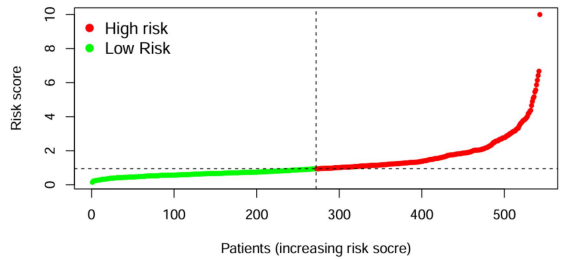
(B)


Hazard ratio
NAXE
PARP10
PTGIS
SLC22A13

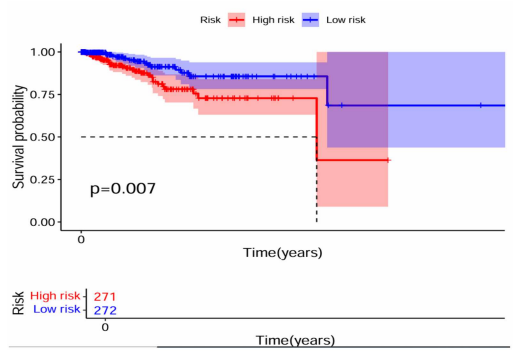
(C)


Dead
Alive
Survival time (years)
0 5 10 15
0 100 200 300 400 500
Patients (increasing risk socre)

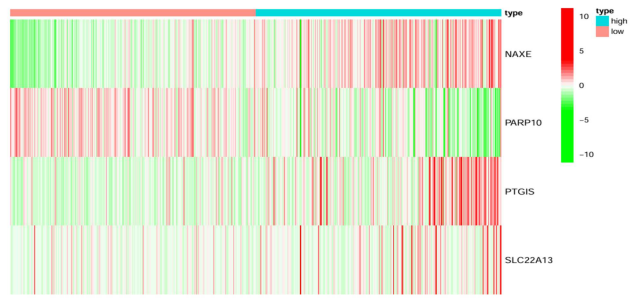
(D)


High risk
Low Risk
Risk score
0 2 4 6 8 10
0 100 200 300 400 500
Patients (increasing risk socre)

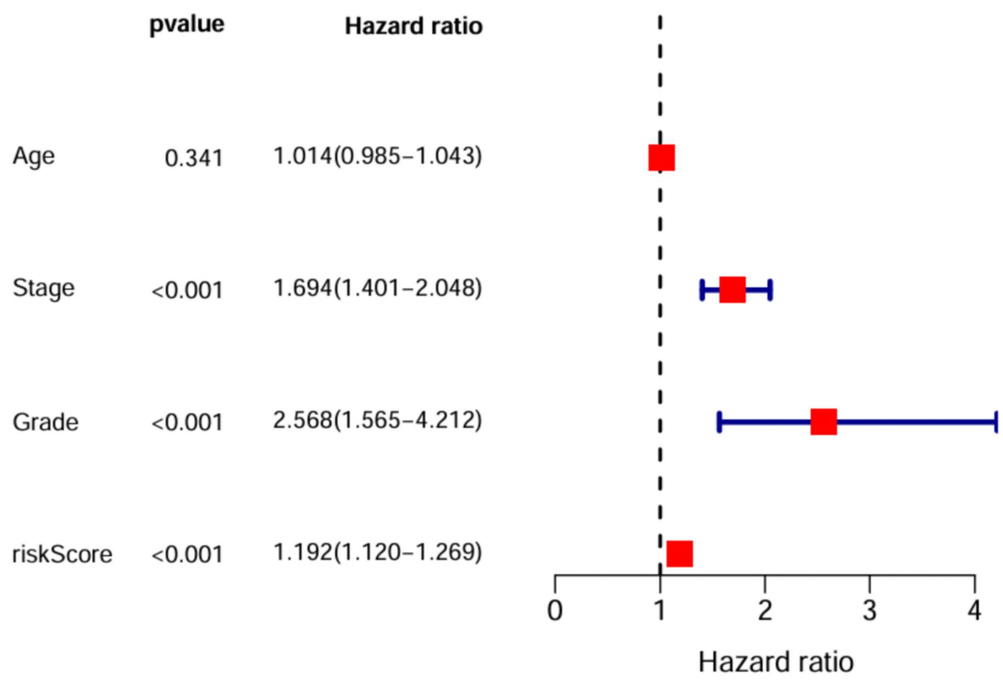
(E)


Risk
High risk
Low risk
Survival probability
1.00
0.75
0.50
0.25
0.00
p=0.007
0
Time(years)
Risk
High risk 271
Low risk 272
0
Time(years)

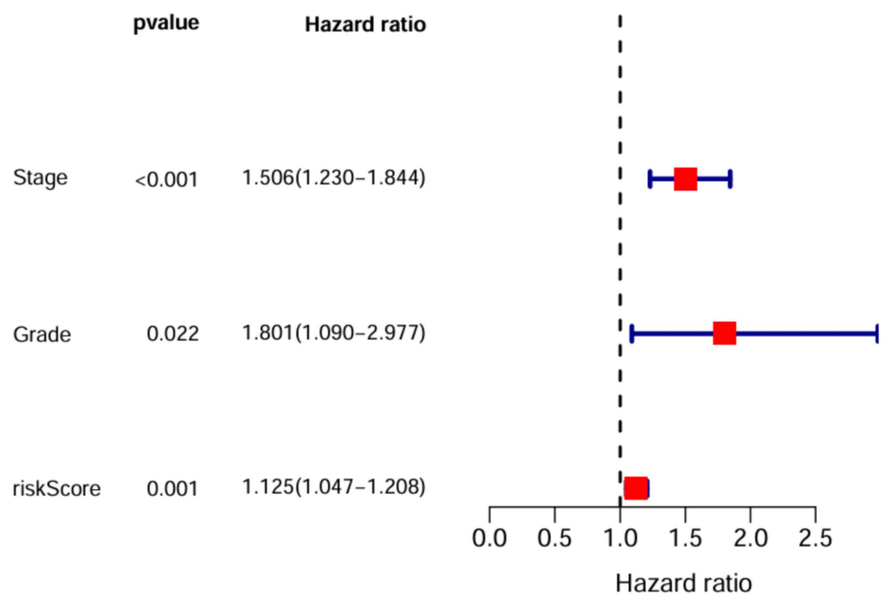
(F)


type
high
low
NAXE
PARP10
PTGIS
SLC22A13
10
5
0
−5
−10

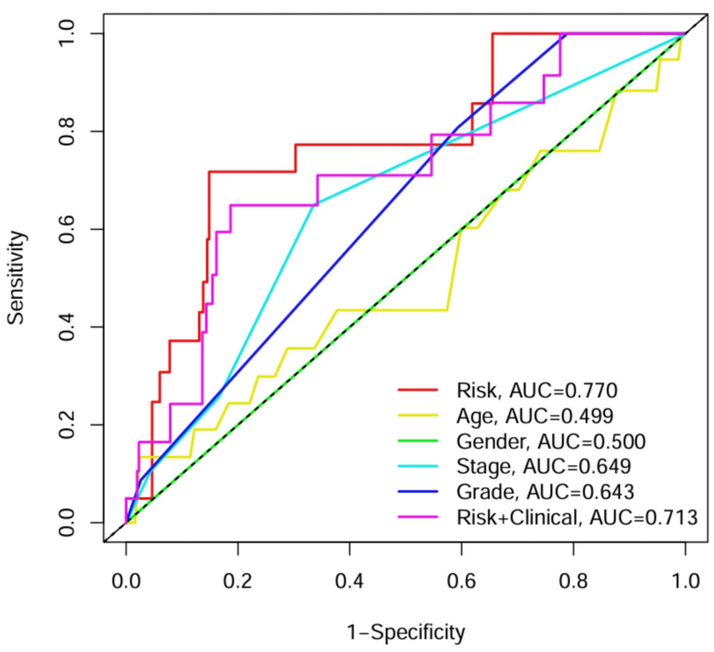
(A)


pvalue
Hazard ratio
Age 0.341 1.014(0.985−1.043)
Stage <0.001 1.694(1.401−2.048)
Grade <0.001 2.568(1.565−4.212)
riskScore <0.001 1.192(1.120−1.269)
0 1 2 3 4
Hazard ratio

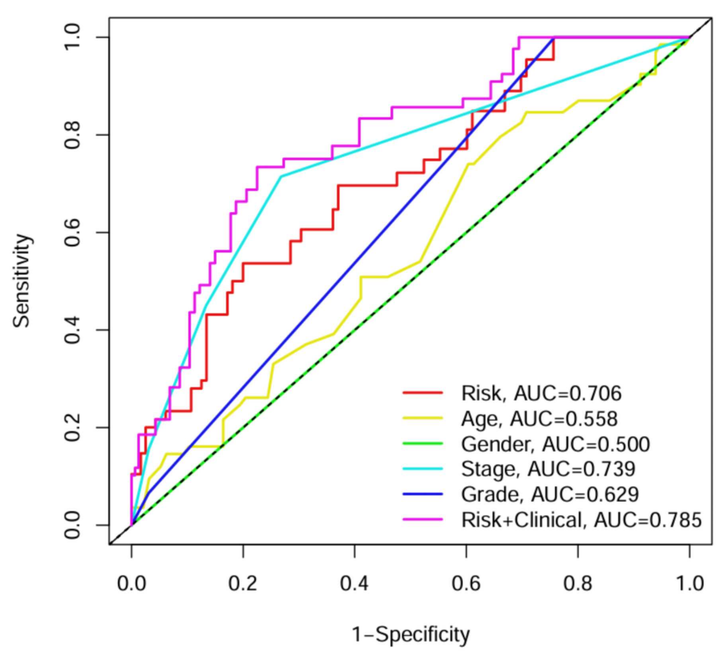
(B)


pvalue
Hazard ratio
Stage <0.001 1.506(1.230−1.844)
Grade 0.022 1.801(1.090−2.977)
riskScore 0.001 1.125(1.047−1.208)
0.0 0.5 1.0 1.5 2.0 2.5
Hazard ratio

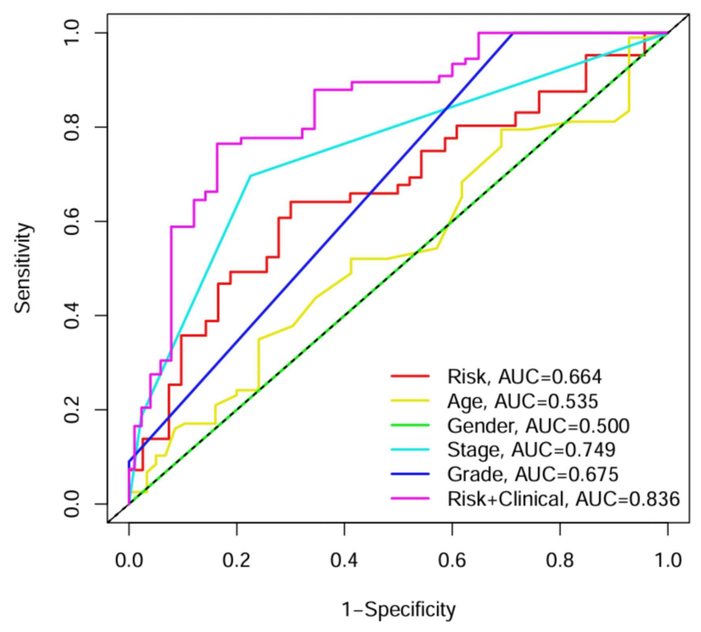
(C)


Sensitivity
1−Specificity
Risk, AUC=0.770
Age, AUC=0.499
Gender, AUC=0.500
Stage, AUC=0.649
Grade, AUC=0.643
Risk+Clinical, AUC=0.713

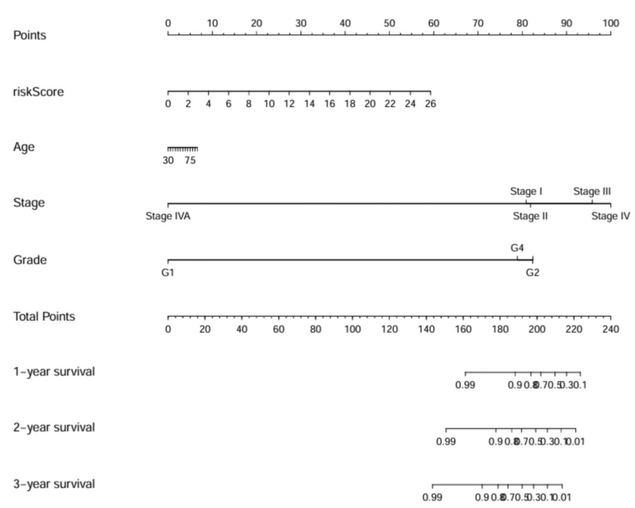
(D)


Sensitivity
1−Specificity
Risk, AUC=0.706
Age, AUC=0.558
Gender, AUC=0.500
Stage, AUC=0.739
Grade, AUC=0.629
Risk+Clinical, AUC=0.785

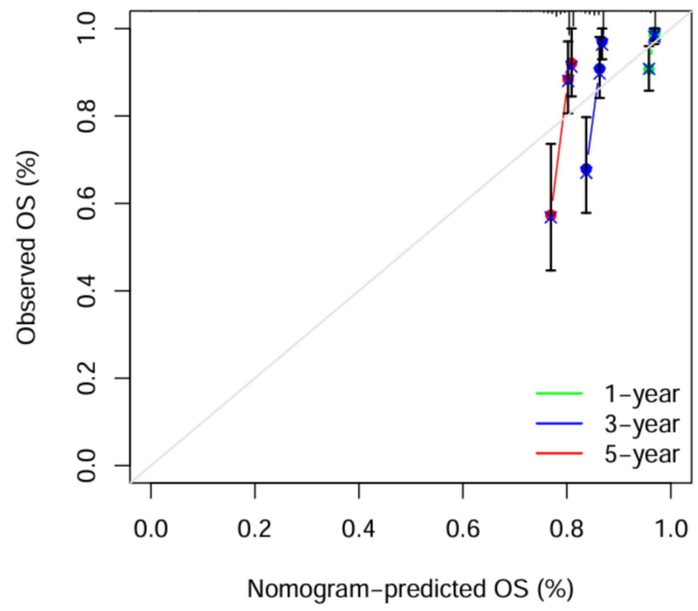
(E)


Sensitivity
1−Specificity
Risk, AUC=0.664
Age, AUC=0.535
Gender, AUC=0.500
Stage, AUC=0.749
Grade, AUC=0.675
Risk+Clinical, AUC=0.836

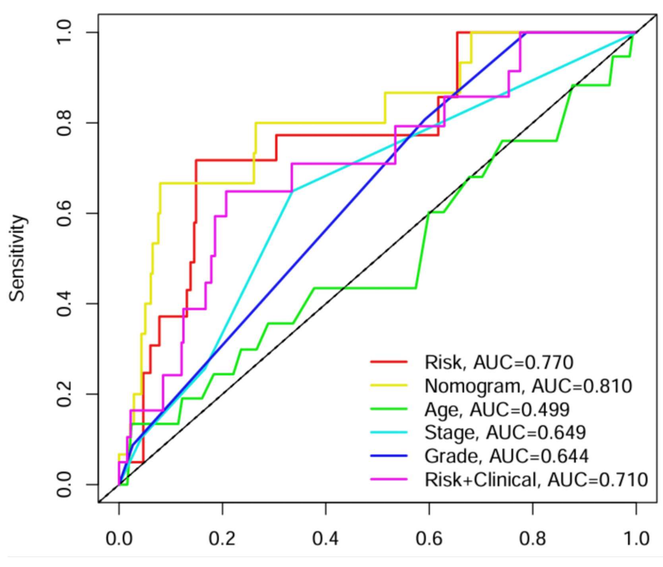
(A)

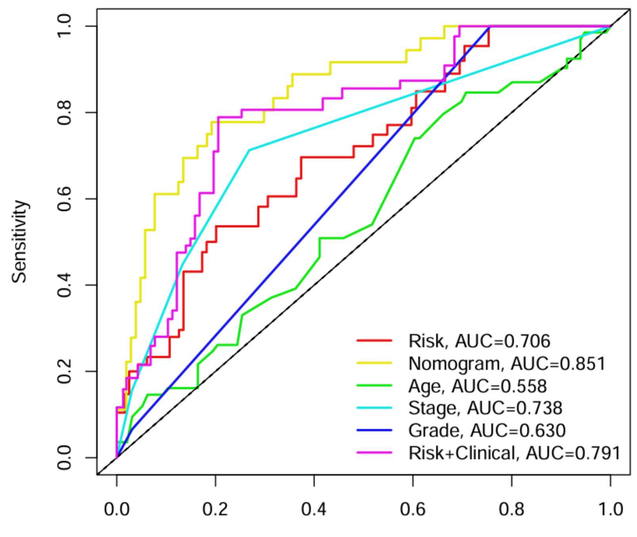

Points
0 10 20 30 40 50 60 70 80 90 100
riskScore
0 2 4 6 8 10 12 14 16 18 20 22 24 26
Age
30 75
Stage
Stage I
Stage III
Stage IVA
Stage II
Stage IV
Grade
G4
G1
G2
Total Points
0 20 40 60 80 100 120 140 160 180 200 220 240
1-year survival
0.99 0.9 0.8 0.7 0.5 0.3 0.1
2-year survival
0.99 0.9 0.8 0.7 0.5 0.3 0.1 0.01
3-year survival
0.99 0.9 0.8 0.7 0.5 0.3 0.1 0.01

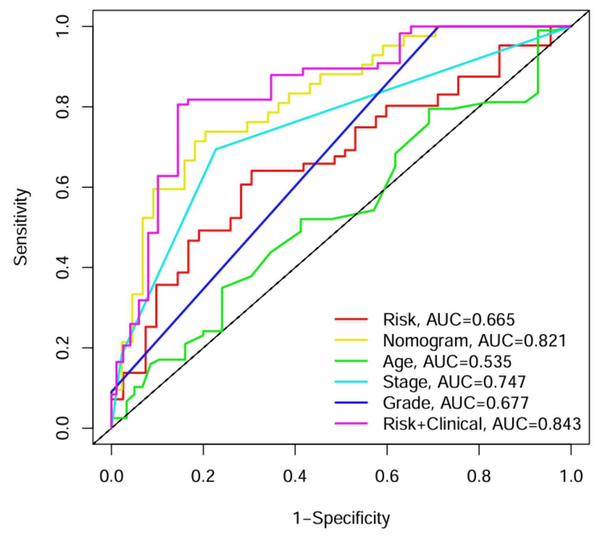
(B)


Observed OS (%)
Nomogram-predicted OS (%)
0.0 0.2 0.4 0.6 0.8 1.0
1-year
3-year
5-year

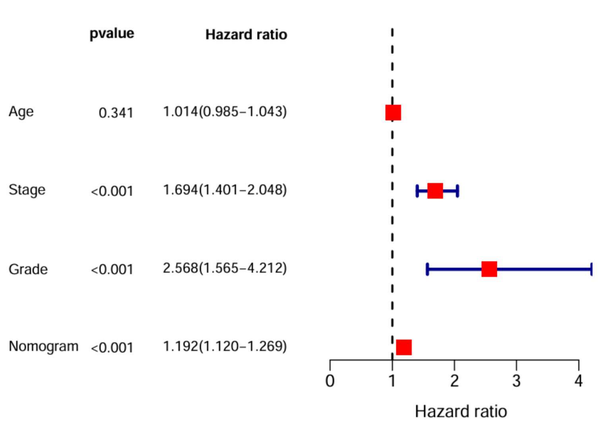
(C)


Sensitivity
0.0 0.2 0.4 0.6 0.8 1.0
Risk, AUC=0.770
Nomogram, AUC=0.810
Age, AUC=0.499
Stage, AUC=0.649
Grade, AUC=0.644
Risk+Clinical, AUC=0.710

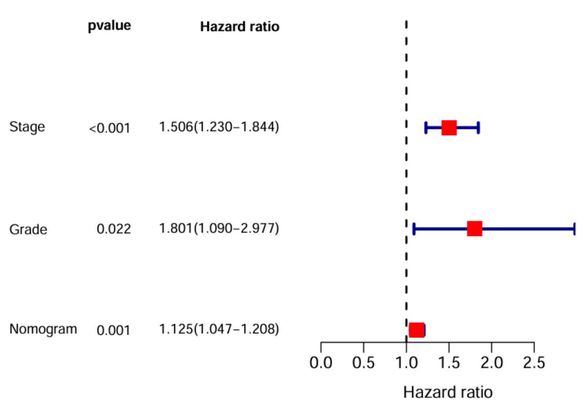

Sensitivity
0.0 0.2 0.4 0.6 0.8 1.0
Risk, AUC=0.706
Nomogram, AUC=0.851
Age, AUC=0.558
Stage, AUC=0.738
Grade, AUC=0.630
Risk+Clinical, AUC=0.791


Sensitivity
1-Specificity
0.0 0.2 0.4 0.6 0.8 1.0
Risk, AUC=0.665
Nomogram, AUC=0.821
Age, AUC=0.535
Stage, AUC=0.747
Grade, AUC=0.677
Risk+Clinical, AUC=0.843

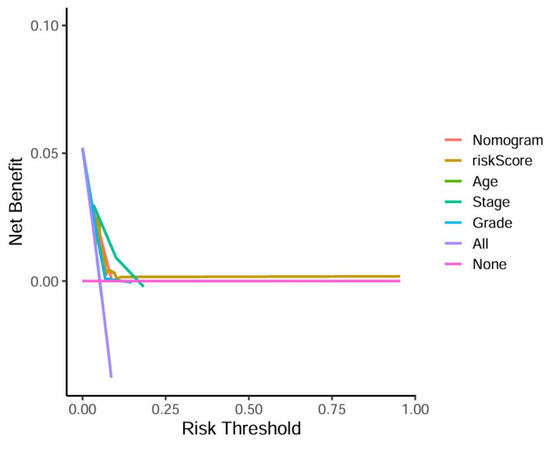
(E)


pvalue
Hazard ratio
Age 0.341 1.014(0.985-1.043)
Stage <0.001 1.694(1.401-2.048)
Grade <0.001 2.568(1.565-4.212)
Nomogram <0.001 1.192(1.120-1.269)
0 1 2 3 4
Hazard ratio

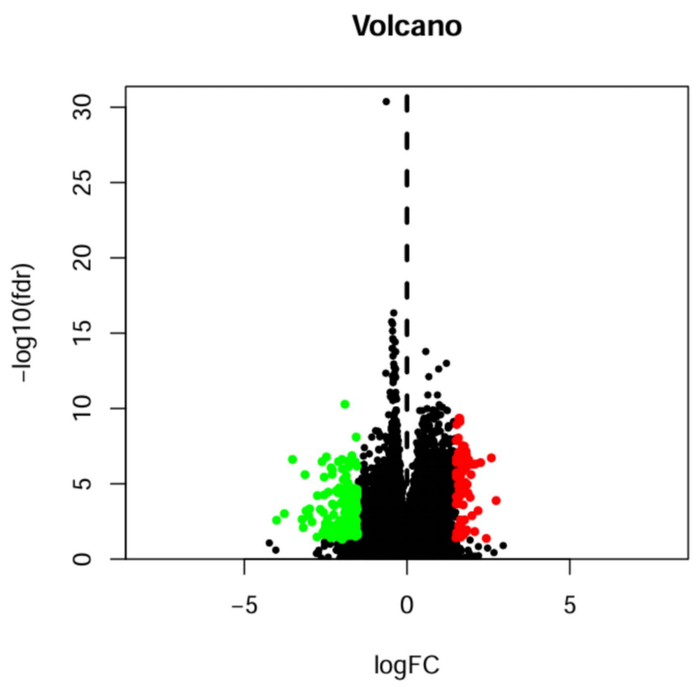
(F)


pvalue
Hazard ratio
Stage <0.001 1.506(1.230-1.844)
Grade 0.022 1.801(1.090-2.977)
Nomogram 0.001 1.125(1.047-1.208)
0.0 0.5 1.0 1.5 2.0 2.5
Hazard ratio

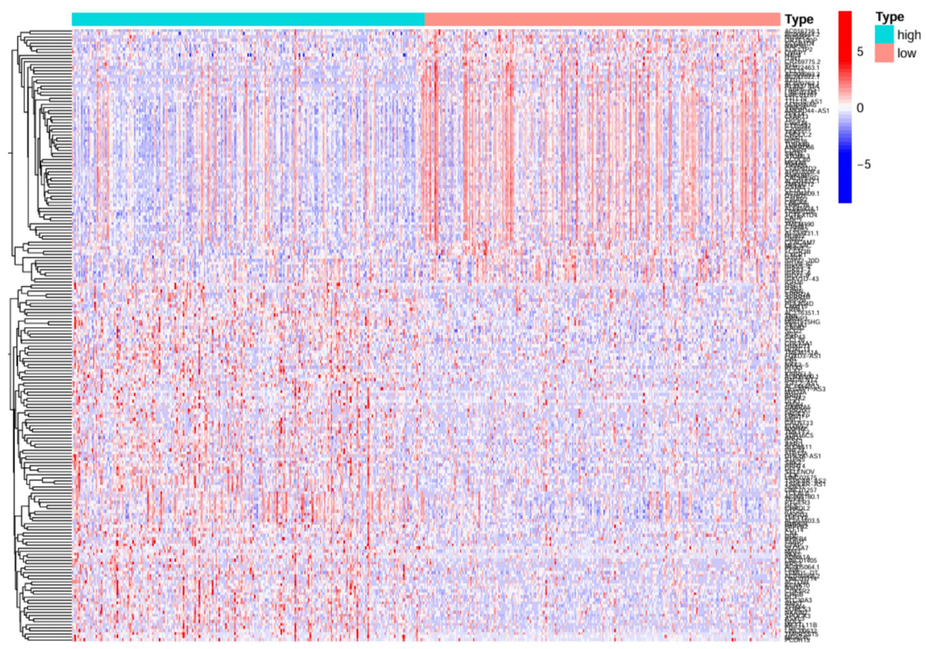
(G)


Net Benefit
0.10
0.05
0.00
0.00 0.25 0.50 0.75 1.00
Risk Threshold
Nomogram
riskScore
Age
Stage
Grade
All
None

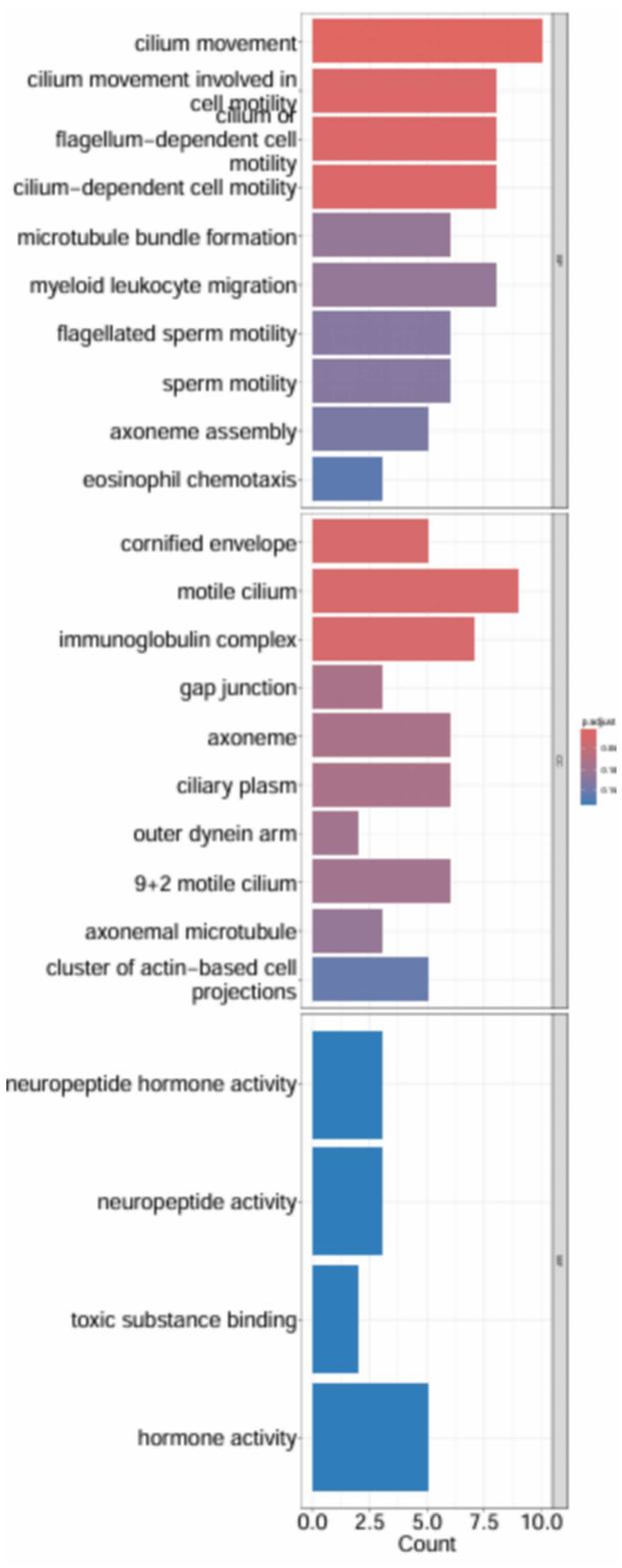
(A)


Volcano
−log10(fdr)
0
5
10
15
20
25
30
−5
0
5
logFC

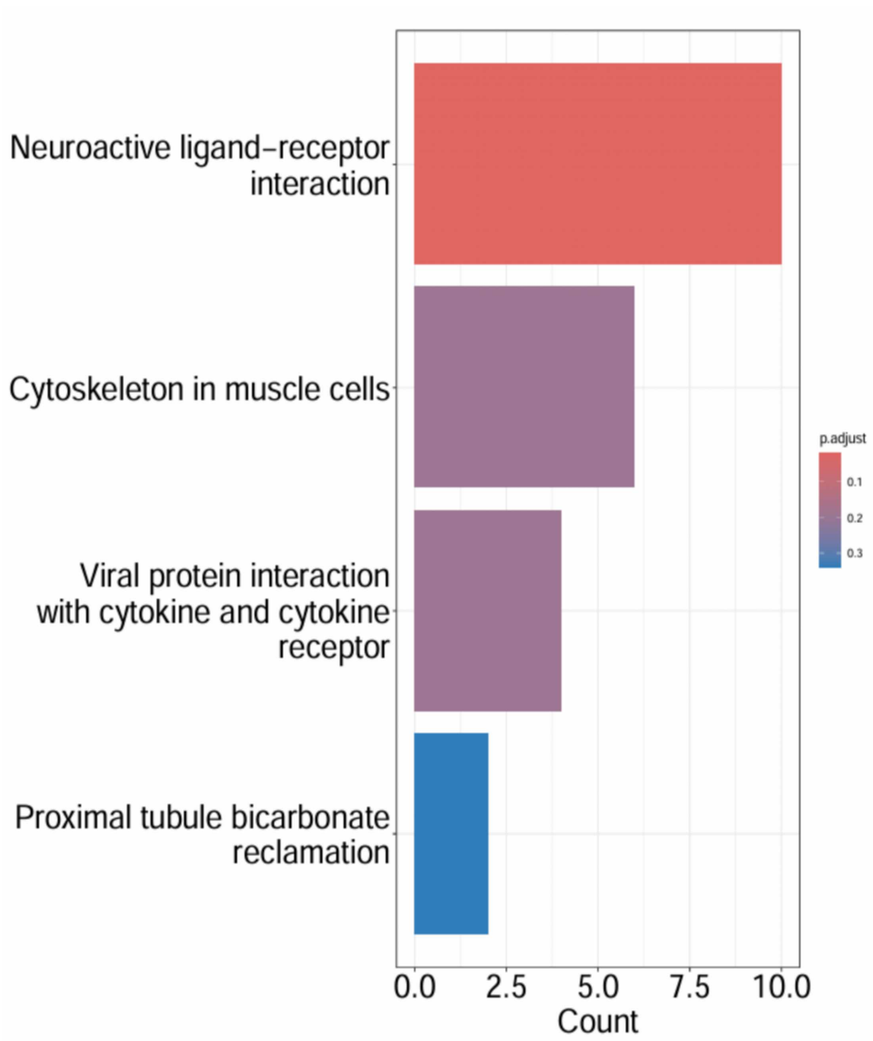
(B)


Type
high
low
5
0
−5

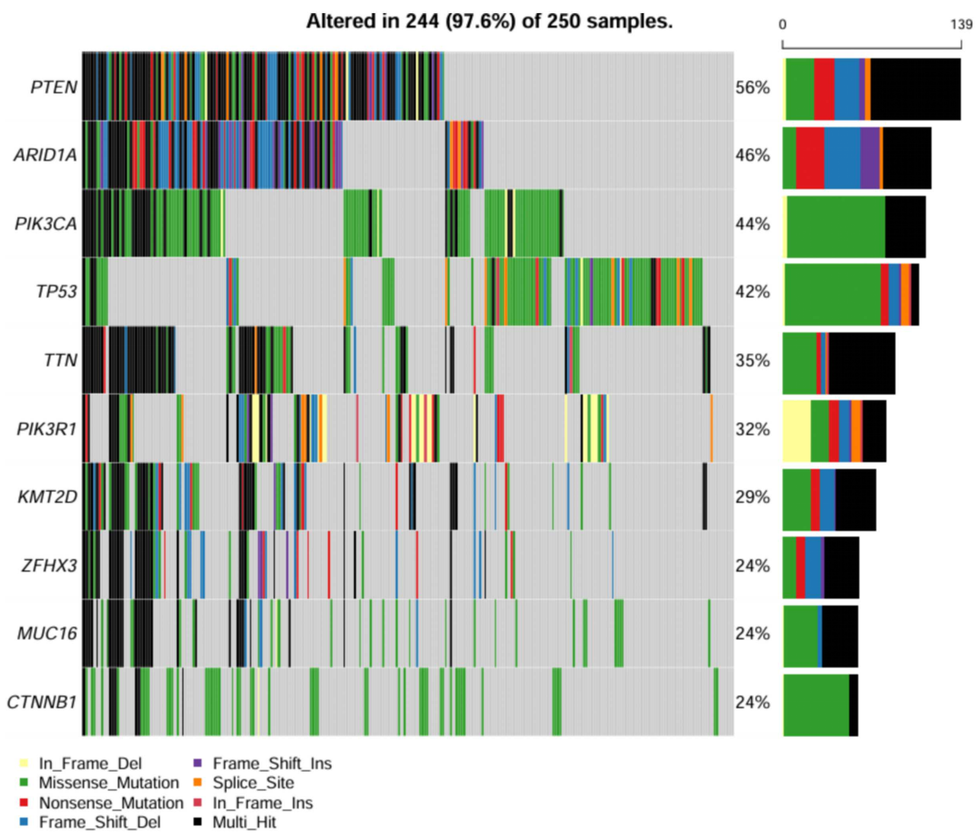
(C)


cilium movement
cilium movement involved in cell motility
cilium or flagellum-dependent cell motility
cilium-dependent cell motility
microtubule bundle formation
myeloid leukocyte migration
flagellated sperm motility
sperm motility
axoneme assembly
eosinophil chemotaxis
cornified envelope
motile cilium
immunoglobulin complex
gap junction
axoneme
ciliary plasm
outer dynein arm
9+2 motile cilium
axonemal microtubule
cluster of actin-based cell projections
neuropeptide hormone activity
neuropeptide activity
toxic substance binding
hormone activity
0.0
2.5
5.0
7.5
10.0
Count

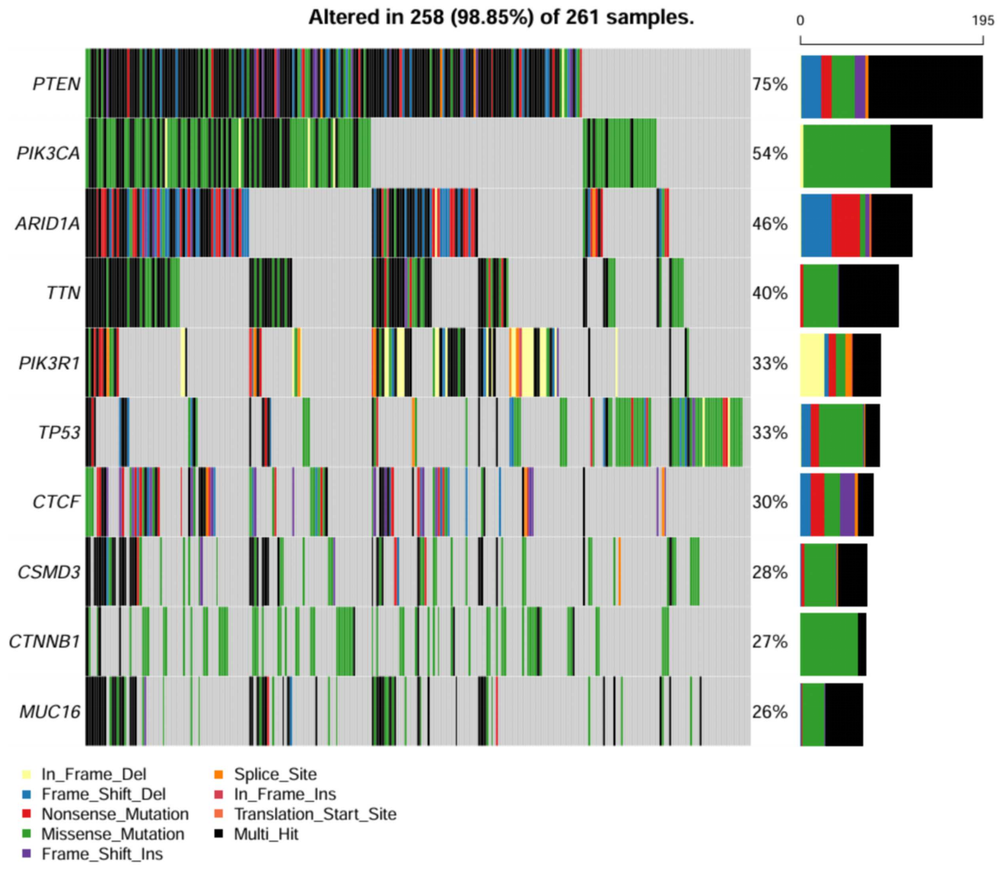
(D)


Neuroactive ligand-receptor interaction
Cytoskeleton in muscle cells
Viral protein interaction with cytokine and cytokine receptor
Proximal tubule bicarbonate reclamation
p.adjust
0.1
0.2
0.3
0.0
2.5
5.0
7.5
10.0
Count

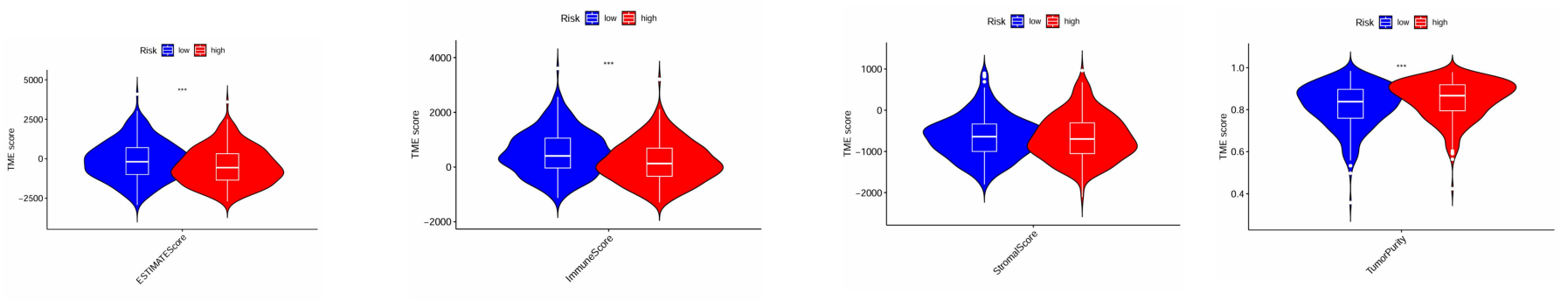
(A)


Altered in 244 (97.6%) of 250 samples.
0
139
PTEN 56%
ARID1A 46%
PIK3CA 44%
TP53 42%
TTN 35%
PIK3R1 32%
KMT2D 29%
ZFHX3 24%
MUC16 24%
CTNNB1 24%
In_Frame_Del
Missense_Mutation
Nonsense_Mutation
Frame_Shift_Del
Frame_Shift_Ins
Splice_Site
In_Frame_Ins
Multi_Hit

(B)


Altered in 258 (98.85%) of 261 samples.
0
195
PTEN 75%
PIK3CA 54%
ARID1A 46%
TTN 40%
PIK3R1 33%
TP53 33%
CTCF 30%
CSMD3 28%
CTNNB1 27%
MUC16 26%
In_Frame_Del
Frame_Shift_Del
Nonsense_Mutation
Missense_Mutation
Frame_Shift_Ins
Splice_Site
In_Frame_Ins
Translation_Start_Site
Multi_Hit

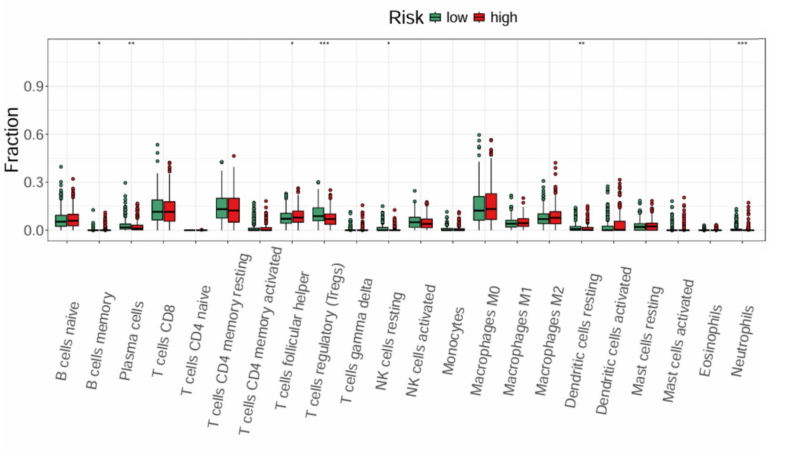
(A)


Risk low high
TME score
ESTIMATEScore
ImmuneScore
StromalScore
TumorPurity

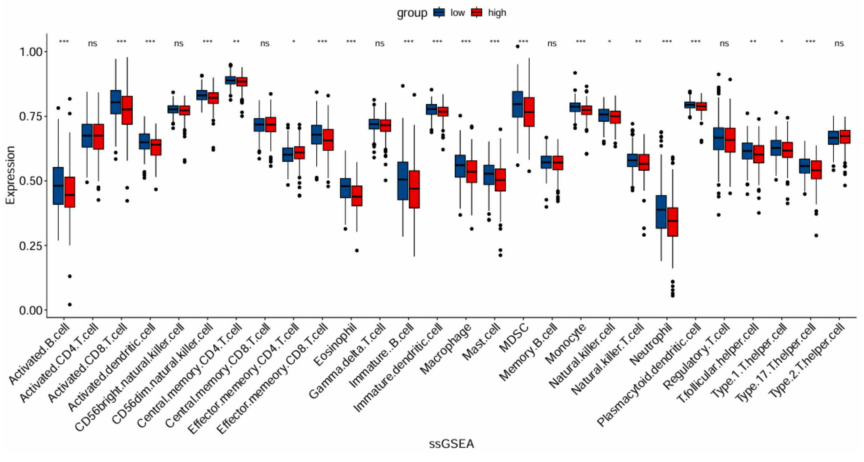
(B)


Estiamted Proportion
Cell Type
B cells memory
B cells naive
Correlation
Dendritic cells activated
Dendritic cells resting
Eosinophils
Macrophages M0
Macrophages M1
Macrophages M2
Mast cells activated
Mast cells resting
Monocytes
Neutrophils
NK cells activated
NK cells resting
P-value
Plasma cells
RMSE
T cells CD4 memory activated
T cells CD4 memory resting
T cells CD4 naive
T cells CD8
T cells follicular helper
T cells gamma delta
T cells regulatory (Tregs)

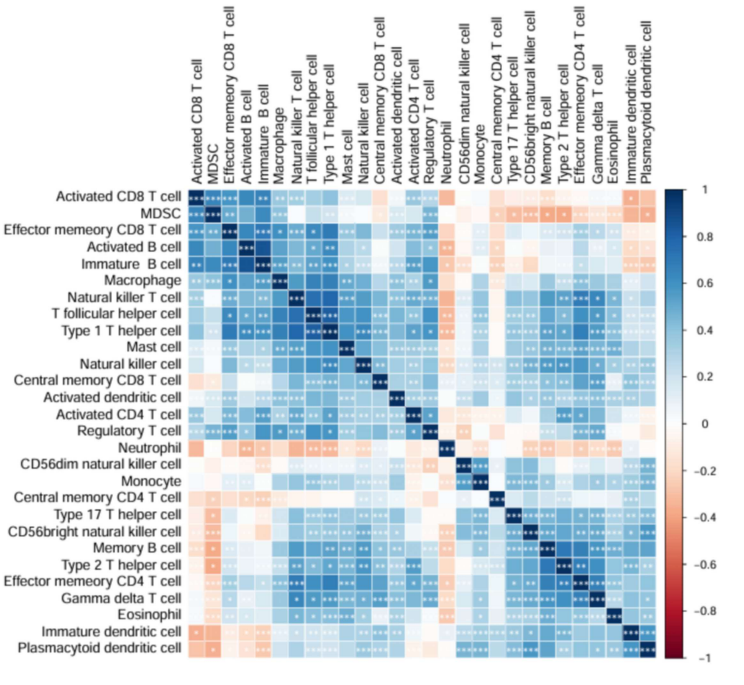
(C)


Risk low high
Fraction
B cells naive
B cells memory
Plasma cells
T cells CD8
T cells CD4 naive
T cells CD4 memory resting
T cells CD4 memory activated
T cells follicular helper
T cells regulatory (Tregs)
T cells gamma delta
NK cells resting
NK cells activated
Monocytes
Macrophages M0
Macrophages M1
Macrophages M2
Dendritic cells resting
Dendritic cells activated
Mast cells resting
Mast cells activated
Eosinophils
Neutrophils

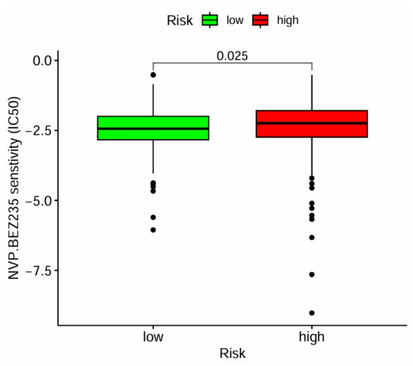
(D)

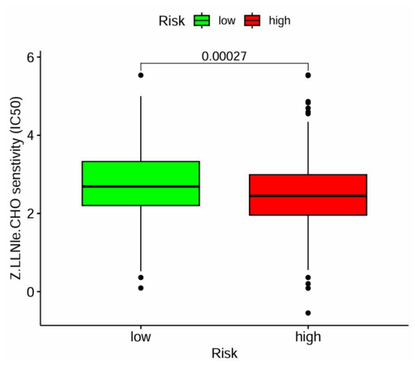

group low high
Expression
ssGSEA
Activated.B.cell
Activated.CD4.T.cell
Activated.CD8.T.cell
Activated.dendritic.cell
CD56bright.natural.killer.cell
CD56dim.natural.killer.cell
Central.memory.CD4.T.cell
Central.memory.CD8.T.cell
Effector.memeory.CD4.T.cell
Effector.memeory.CD8.T.cell
Eosinophil
Gamma.delta.T.cell
Immature..B.cell
Immature.dendritic.cell
Macrophage
Mast.cell
MDSC
Memory.B.cell
Monocyte
Natural.killer.cell
Natural.killer.T.cell
Neutrophil
Plasmacytoid.dendritic.cell
Regulatory.T.cell
T.follicular.helper.cell
Type.1.T.helper.cell
Type.17.T.helper.cell
Type.2.T.helper.cell

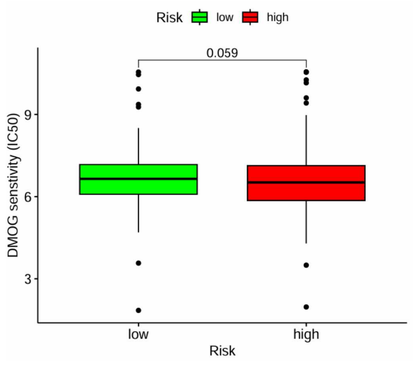
(E)

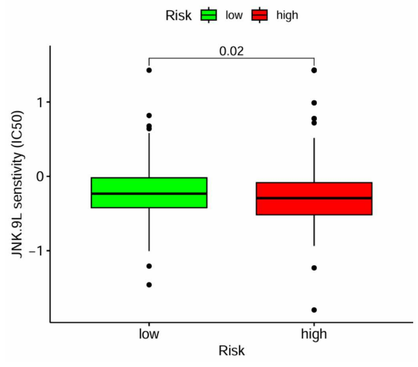

Activated CD8 T cell
MDSC
Effector memeory CD8 T cell
Activated B cell
Immature B cell
Macrophage
Natural killer T cell
T follicular helper cell
Type 1 T helper cell
Mast cell
Natural killer cell
Central memory CD8 T cell
Activated dendritic cell
Activated CD4 T cell
Regulatory T cell
Neutrophil
CD56dim natural killer cell
Monocyte
Central memory CD4 T cell
Type 17 T helper cell
CD56bright natural killer cell
Memory B cell
Type 2 T helper cell
Effector memeory CD4 T cell
Gamma delta T cell
Eosinophil
Immature dendritic cell
Plasmacytoid dendritic cell

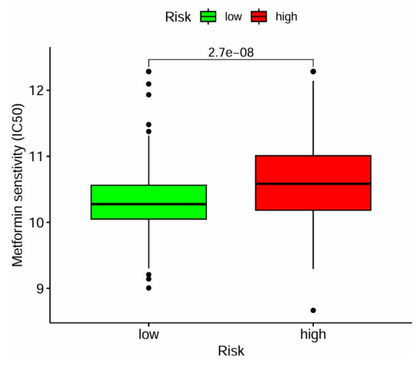
(A)

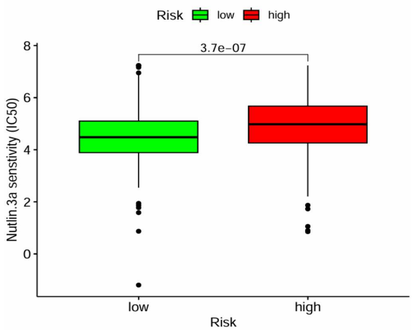


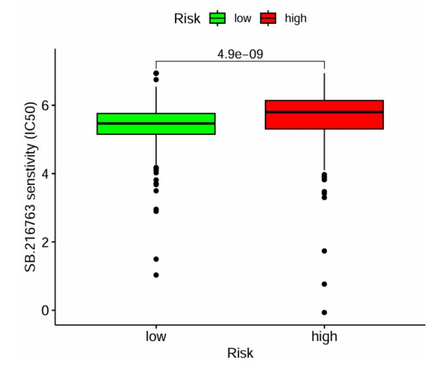


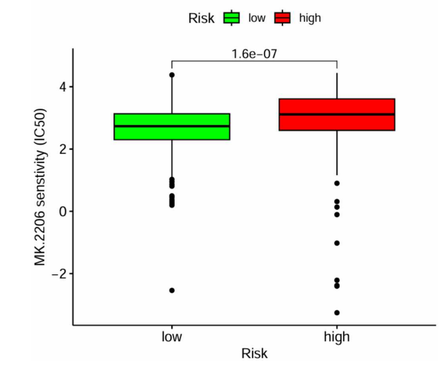


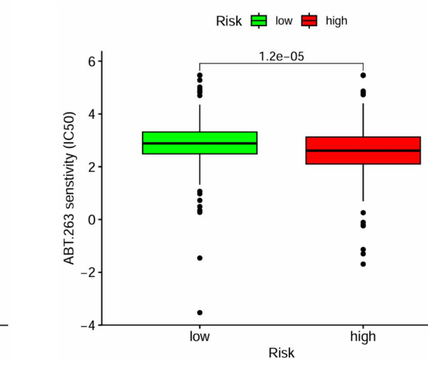


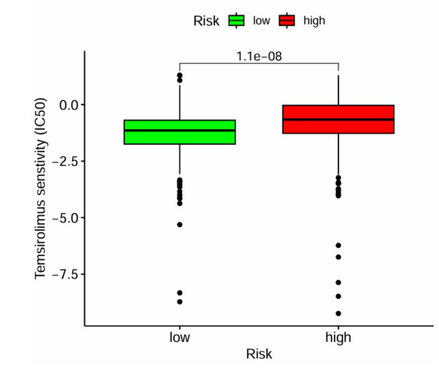


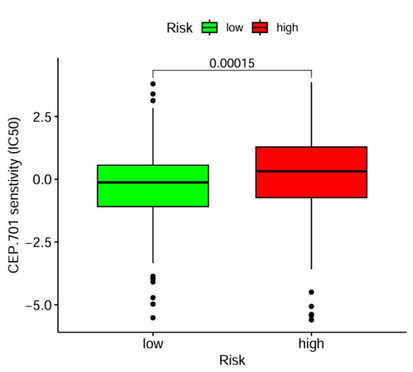










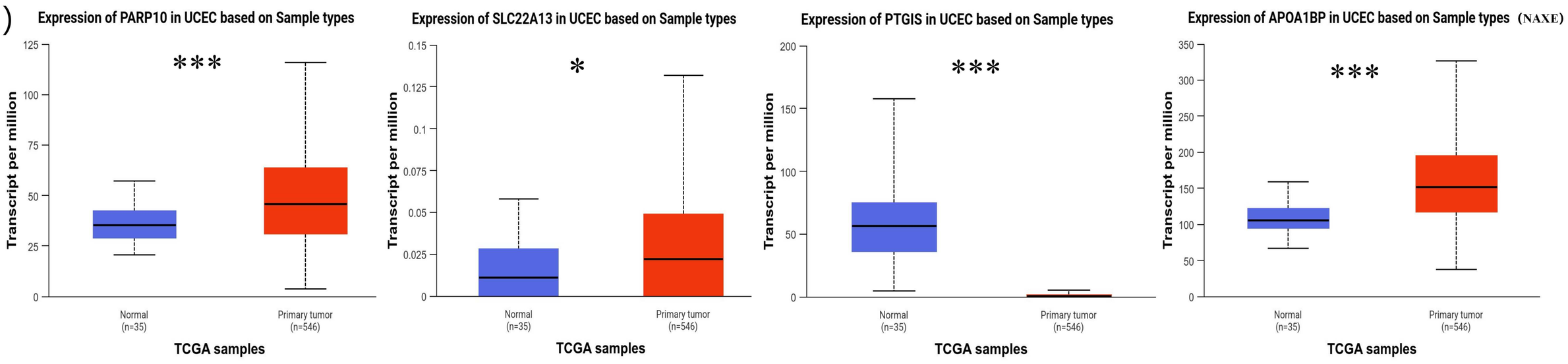


(B)

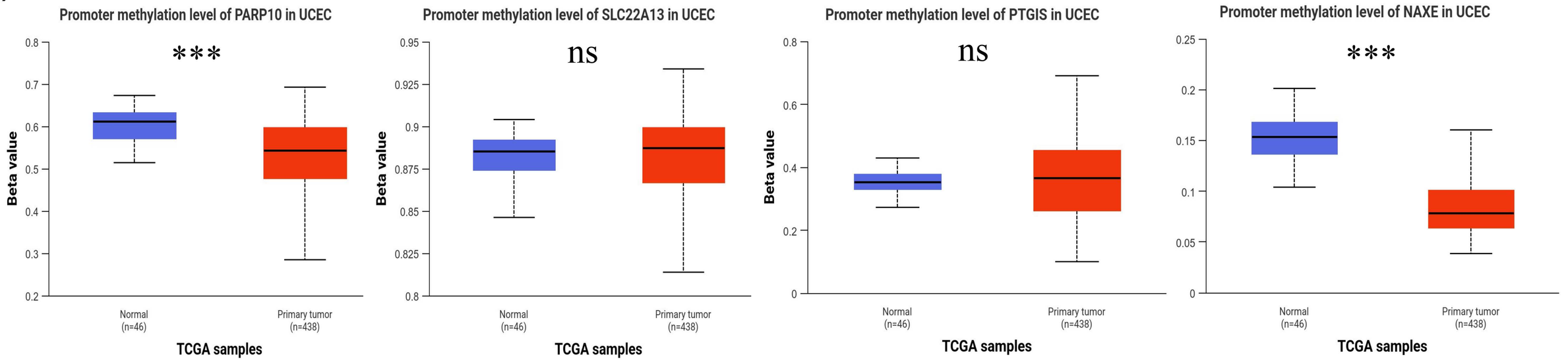
	Physicochemical Property		Absorption		Distribution	Excretion	Toxicity
	Log S	Log P	F(20%)	Caco-2	BBB	T1/2	FDAMDD
NVP.BEZ235	-6.695	5.581	---	-4.954	--	0.225	+++
Z.LLNIe.CHO	-4.797	4.869	---	-5.052	++	0.771	++
DMOG	-0.266	-0.465	--	-4.779	+++	0.884	---
JNK.9L	-5.663	4.535	---	-4.882	---	0.103	--
Metformin	-1.163	-1.584	---	-5.745	--	0.369	---
Nutlin.3a	-5.329	5.388	---	-4.993	-	0.044	+
SB.216763	-6.432	4.267	---	-4.894	--	0.062	+++
MK.2206	-4.44	4.813	---	-5.253	-	0.129	+++
ABT.263	-5.62	8.011	---	-5.605	---	0.001	+++
Temsirolimu	-4.117	4.283	++	-4.891	---	0.033	+++
CEP.701	-6.905	4.719	---	-5.718	--	0.06	+++

Excellent Medium Poor

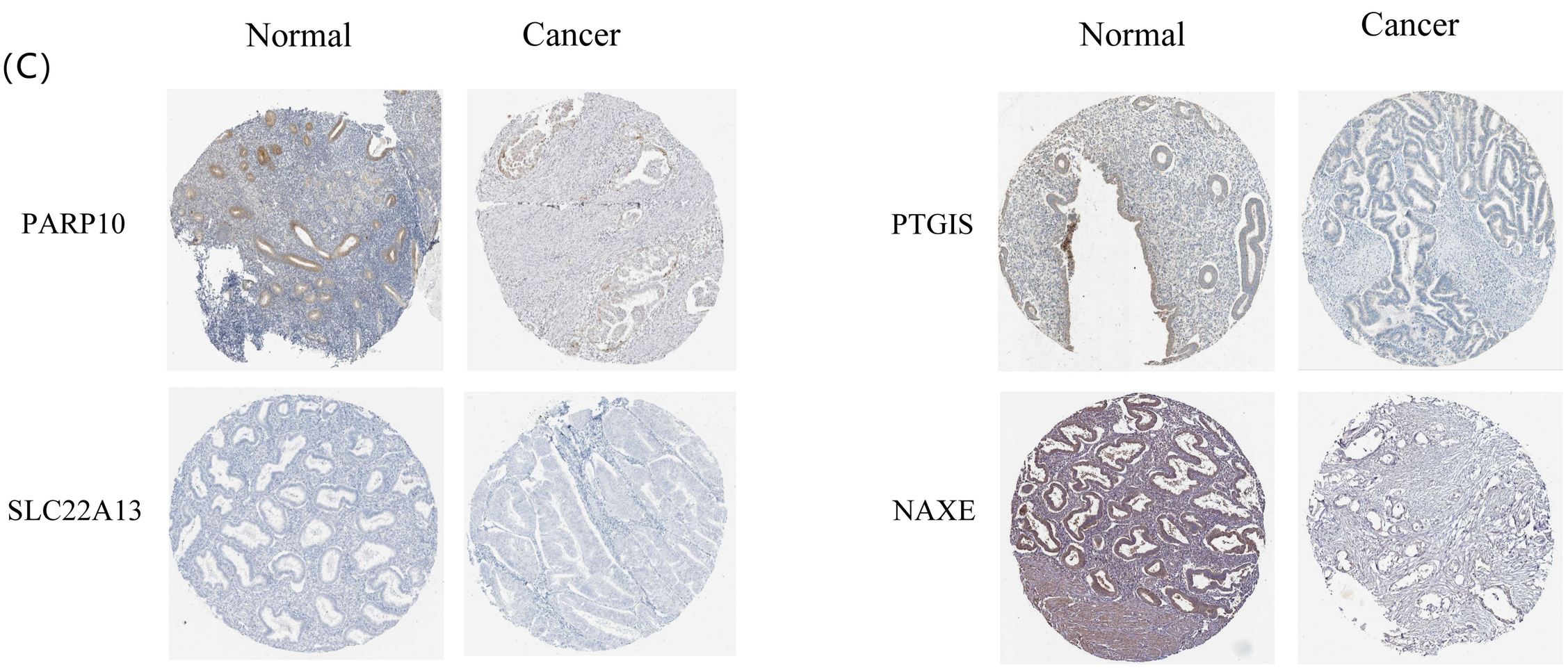
(A)


Expression of PARP10 in UCEC based on Sample types
Transcript per million
***
Normal (n=35)
Primary tumor (n=546)
TCGA samples
Expression of SLC22A13 in UCEC based on Sample types
*
Expression of PTGIS in UCEC based on Sample types
***
Expression of APOA1BP in UCEC based on Sample types (NAXE)
***

(B)


Promoter methylation level of PARP10 in UCEC
Beta value
***
Normal (n=46)
Primary tumor (n=438)
TCGA samples
Promoter methylation level of SLC22A13 in UCEC
ns
Promoter methylation level of PTGIS in UCEC
ns
Promoter methylation level of NAXE in UCEC
***

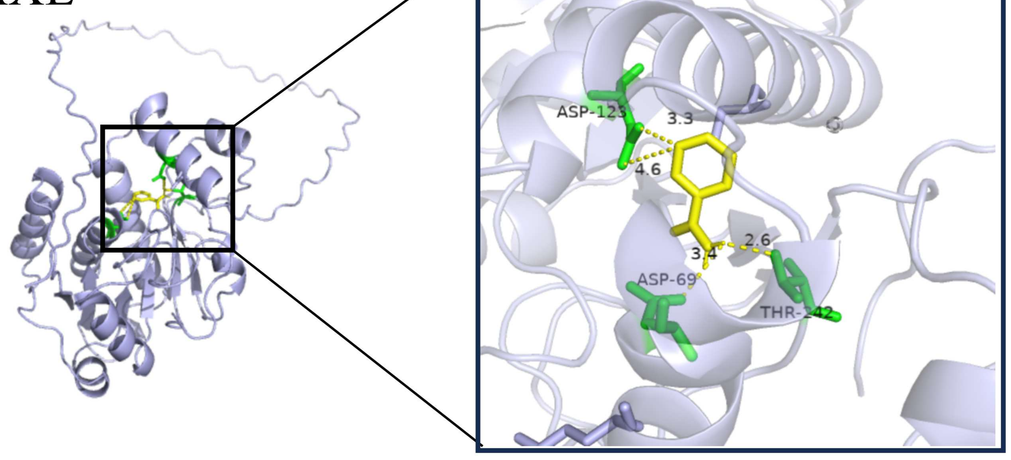
(C)


Normal
Cancer
Normal
Cancer
PARP10
PTGIS
SLC22A13
NAXE

(A)

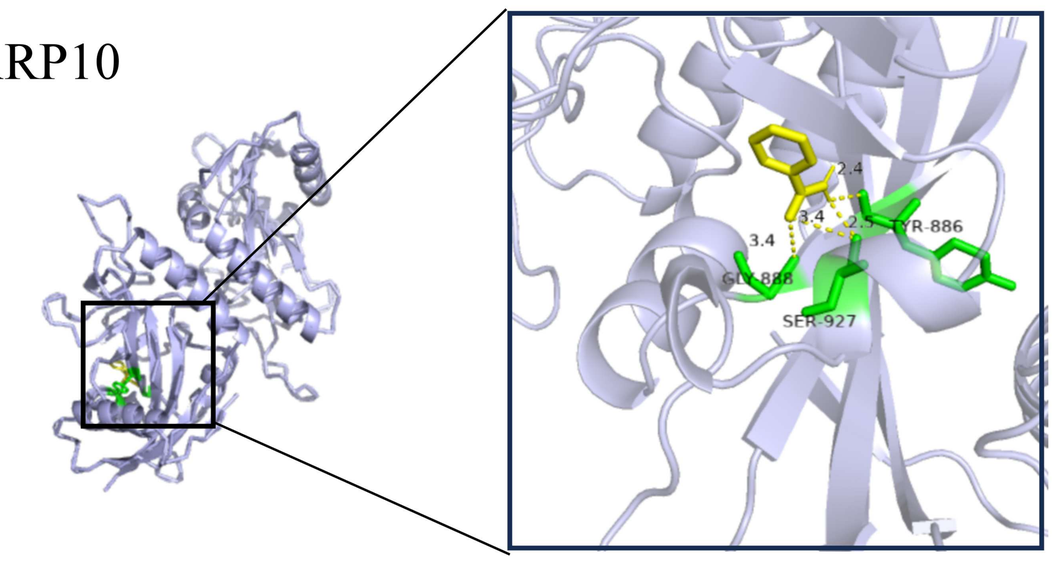
NAXE

BE:-4.919



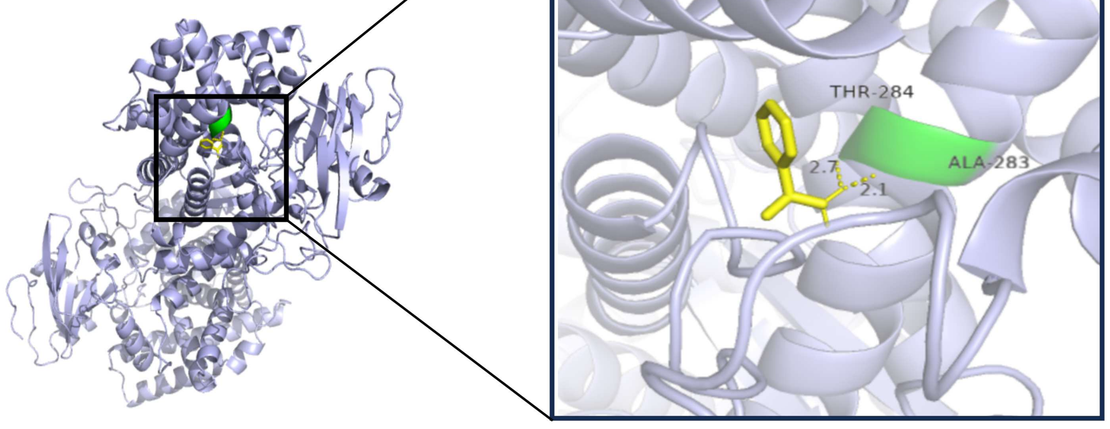
PARP10

BE:-5.574



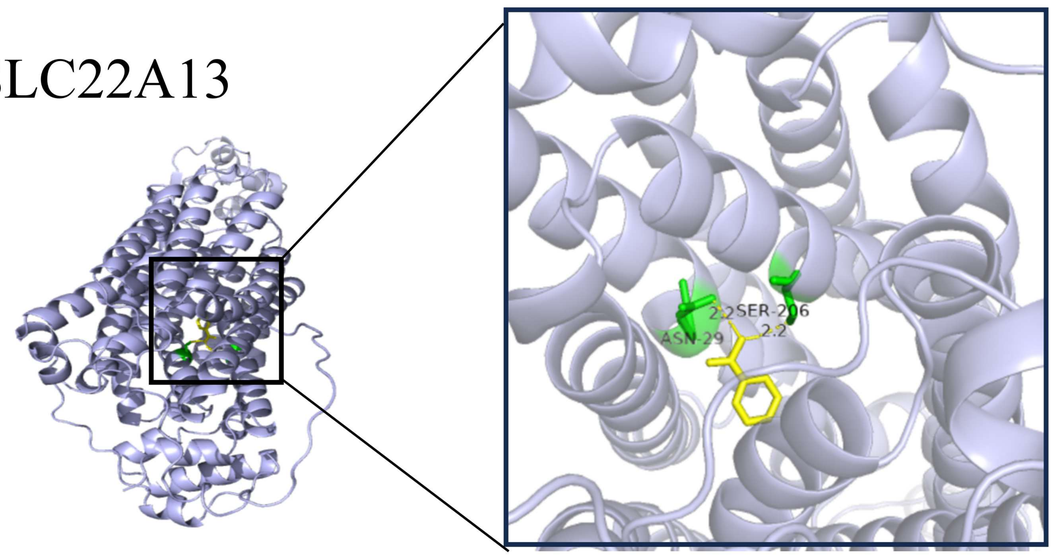
PTGIS

BE： -4.583

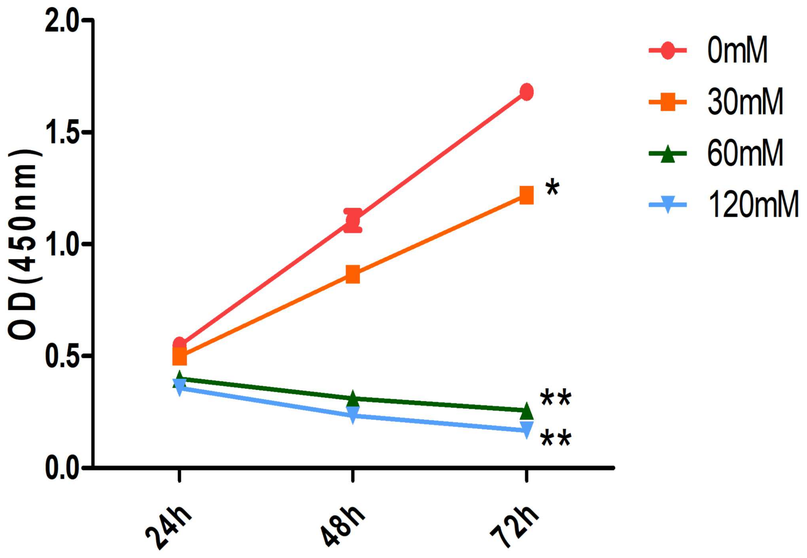


SLC22A13

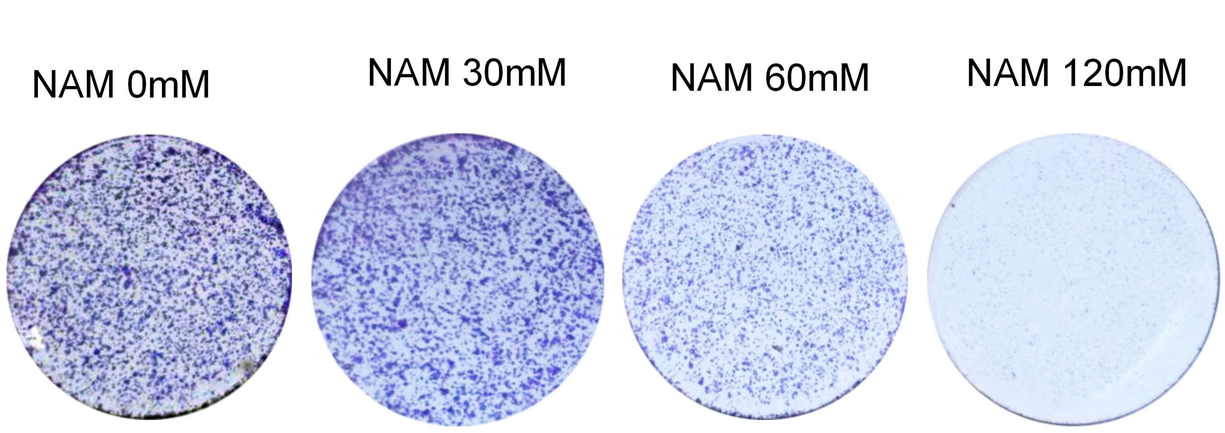
BE:-4.669

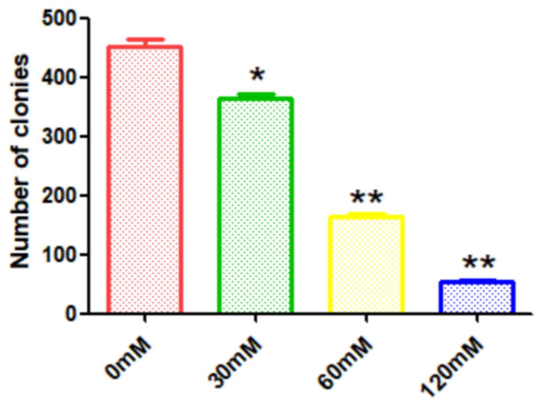


(B)

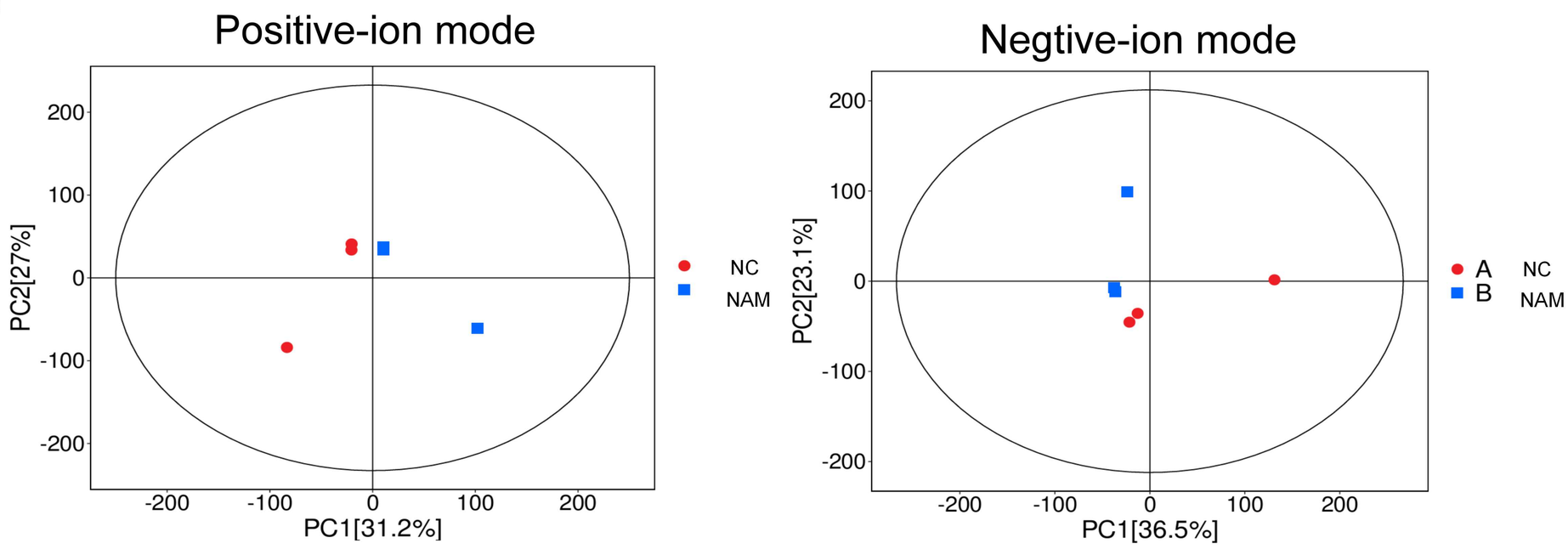


(C)

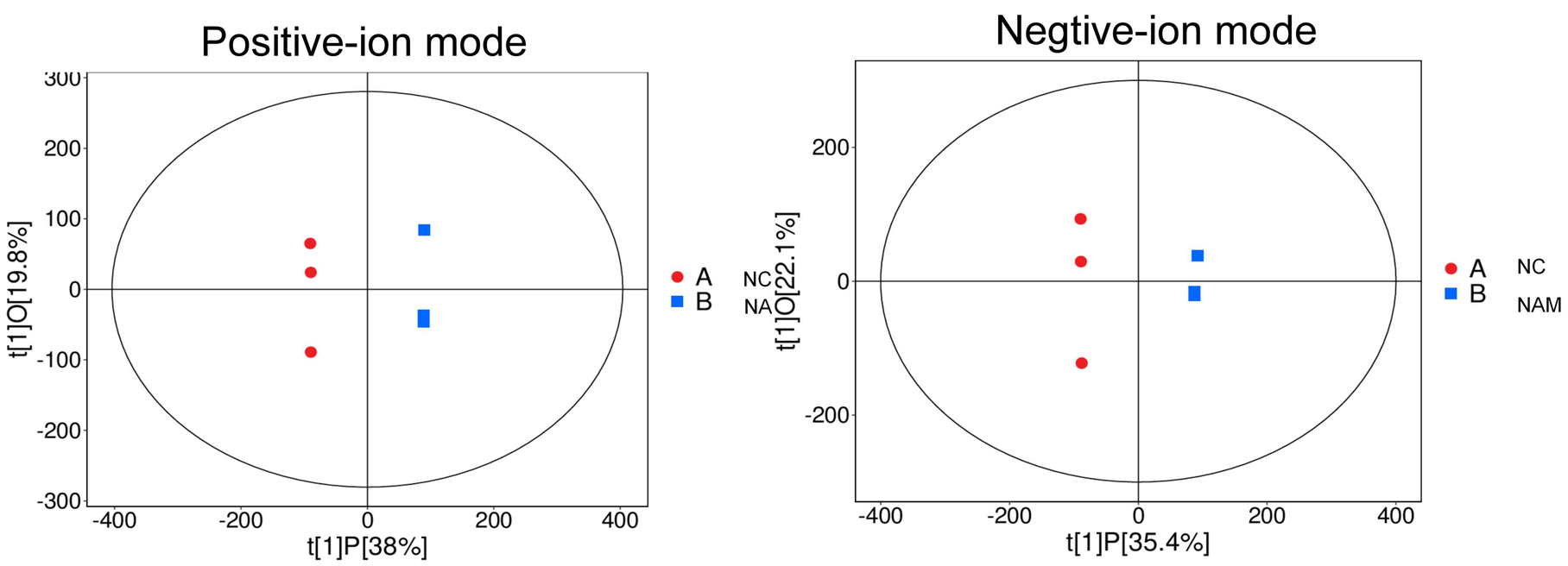




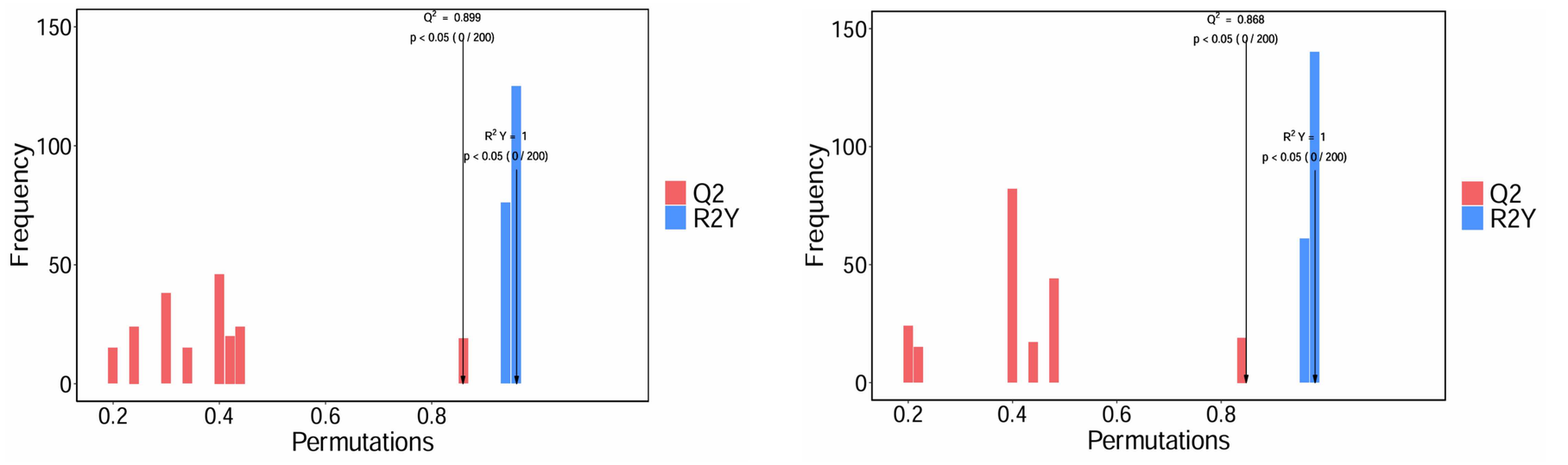
(A)


Positive-ion mode
PC2[27%]
PC1[31.2%]
NC
NAM
Negtive-ion mode
PC2[23.1%]
PC1[36.5%]
A
B
NC
NAM

(B)

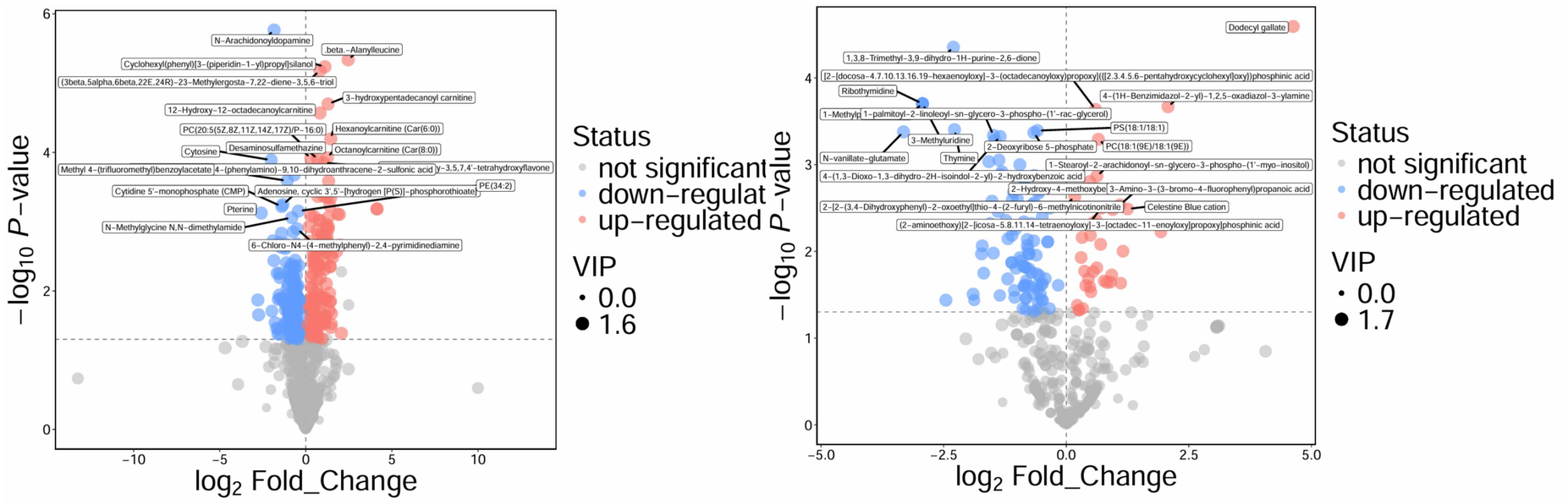

Positive-ion mode
t[1]O[19.8%]
t[1]P[38%]
A
B
NC
NAM
Negtive-ion mode
t[1]O[22.1%]
t[1]P[35.4%]
A
B
NC
NAM

(C)


Frequency
Permutations
Q² = 0.899
p < 0.05 (0 / 200)
R² Y = 1
p < 0.05 (0 / 200)
Q2
R2Y
Frequency
Permutations
Q² = 0.868
p < 0.05 (0 / 200)
R² Y = 1
p < 0.05 (0 / 200)
Q2
R2Y

(A)

Positive-ion mode

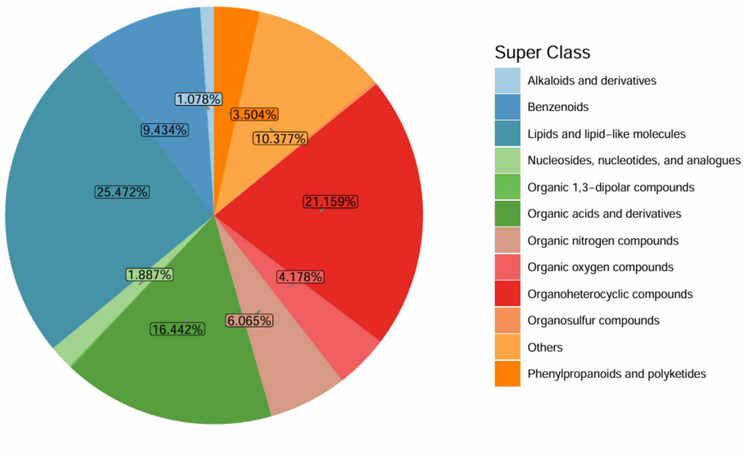


(B)

Negtive-ion mode

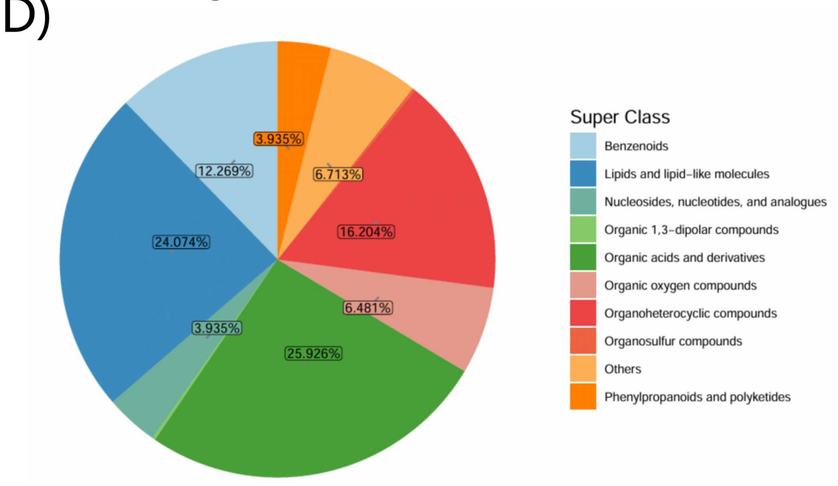
(C)

Positive-ion mode



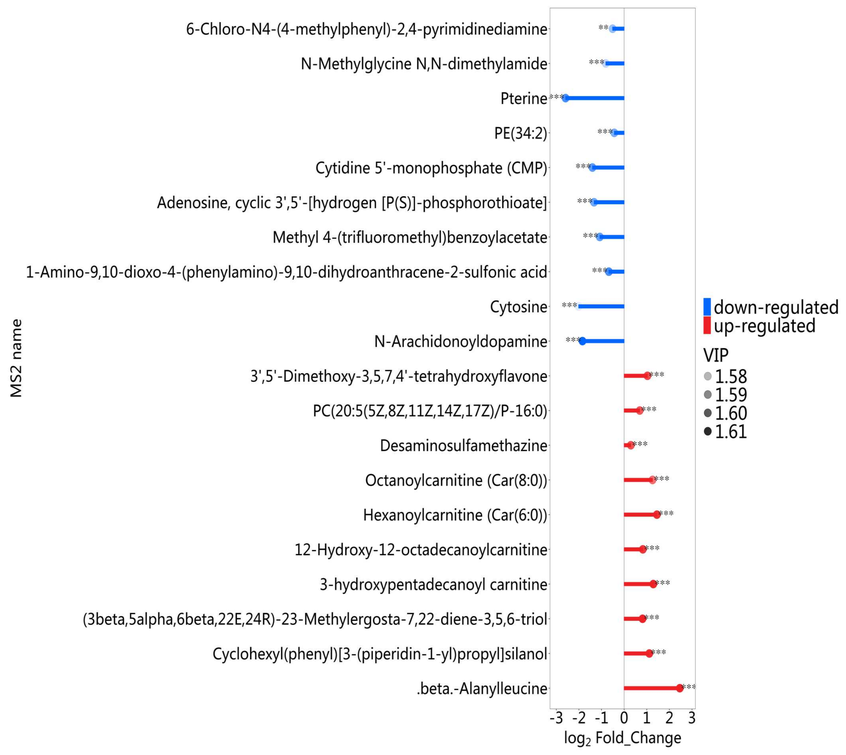
(D)

Negtive-ion mode



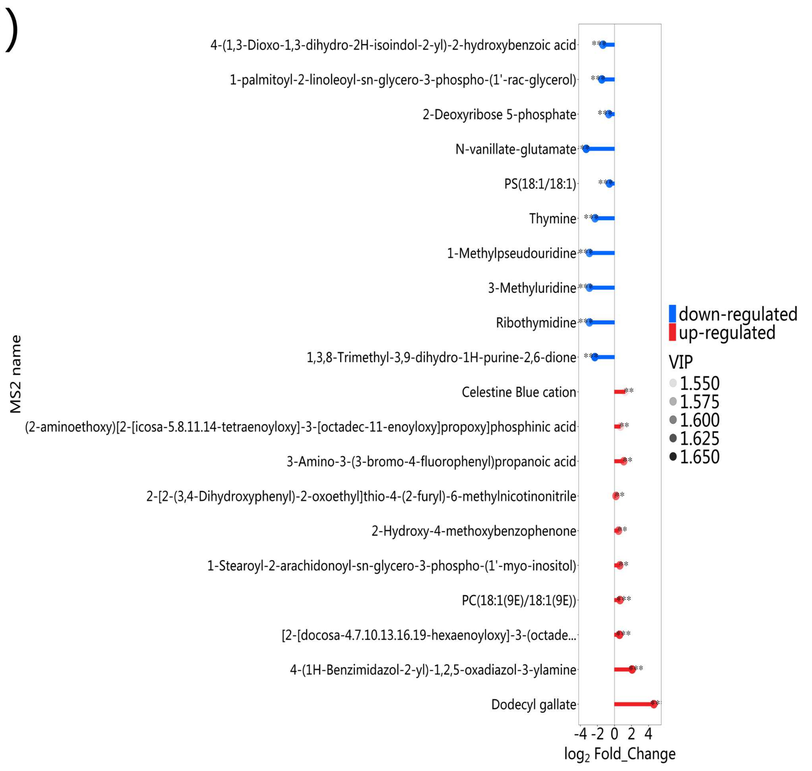
(E)

Positive-ion mode



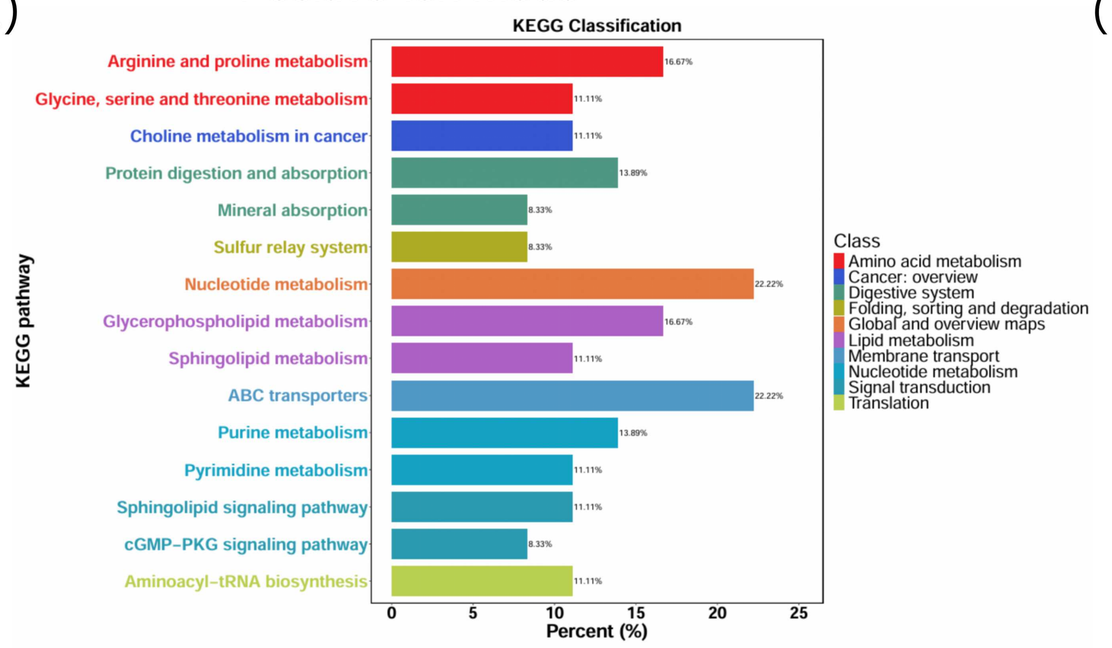
(F)

Negtive-ion mode



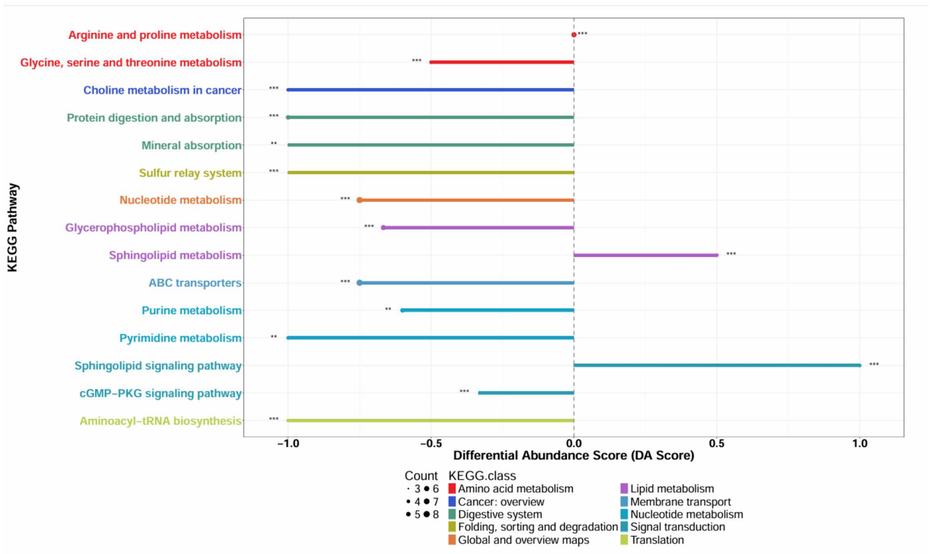
(A)

Positive-ion mode



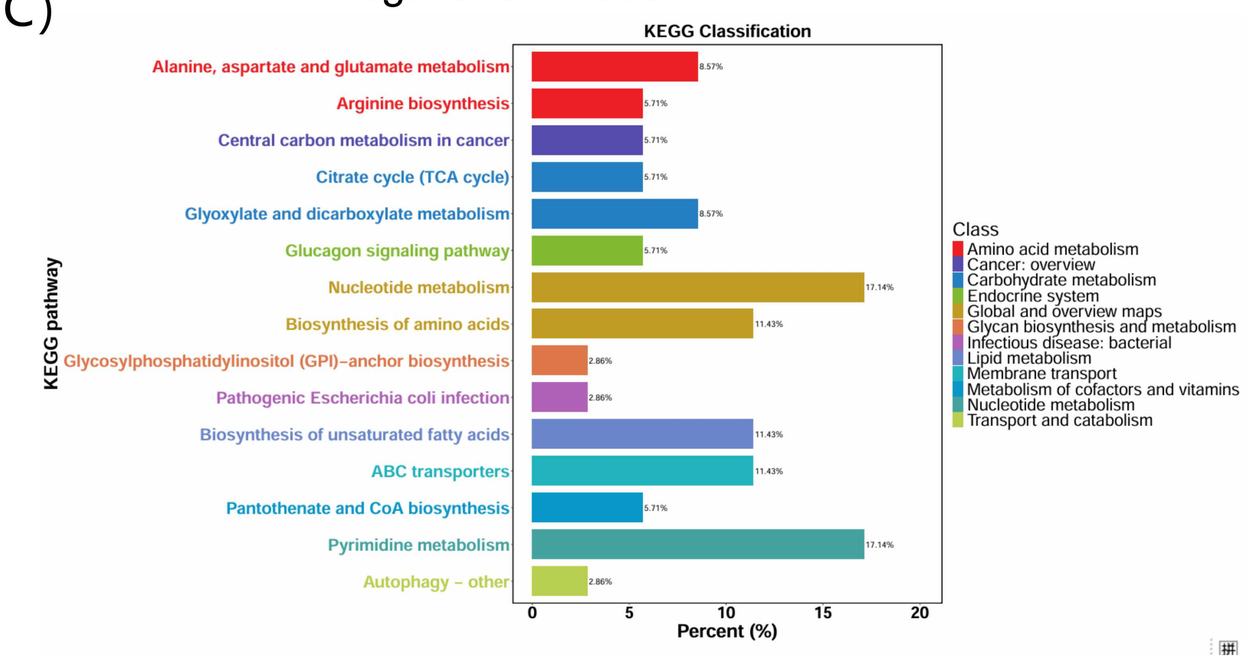
(B)

Positive-ion mode



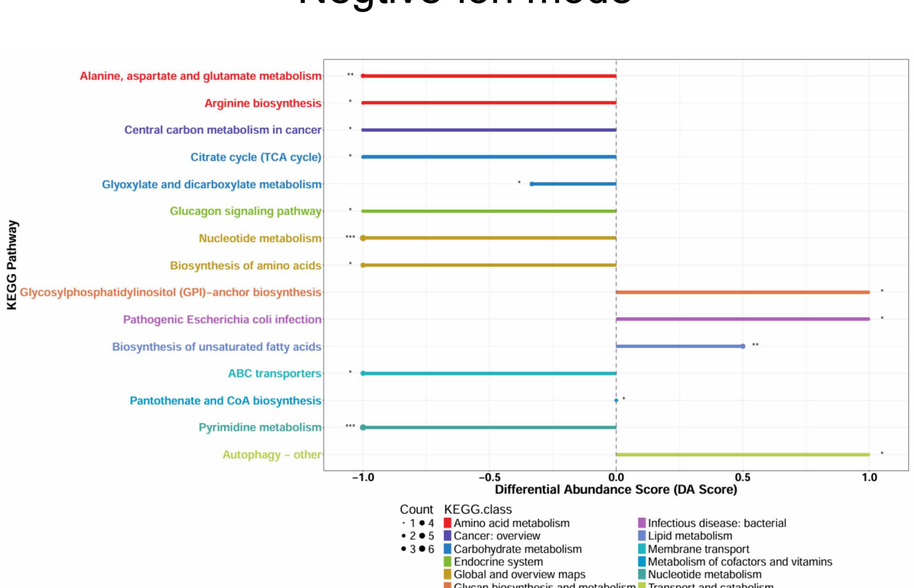
(C)

Negtive-ion mode



(D)

Negtive-ion mode



Supplementary Files

This is a list of supplementary files associated with this preprint. Click to download.

- SupplementFigure1.png
- SupplementFigure2.png
- SupplementFigure3.png
- SupplementFigure4.png
- SupplementaryTableS1.docx
- SupplementaryTableS2.xlsx
- SupplementaryTableS3.xlsx
- SupplementaryDateS1.zip